Article

Cell Systems

Combinatorial interpretation of BMP and WNT controls the decision between primitive streak and extraembryonic fates

Graphical abstract

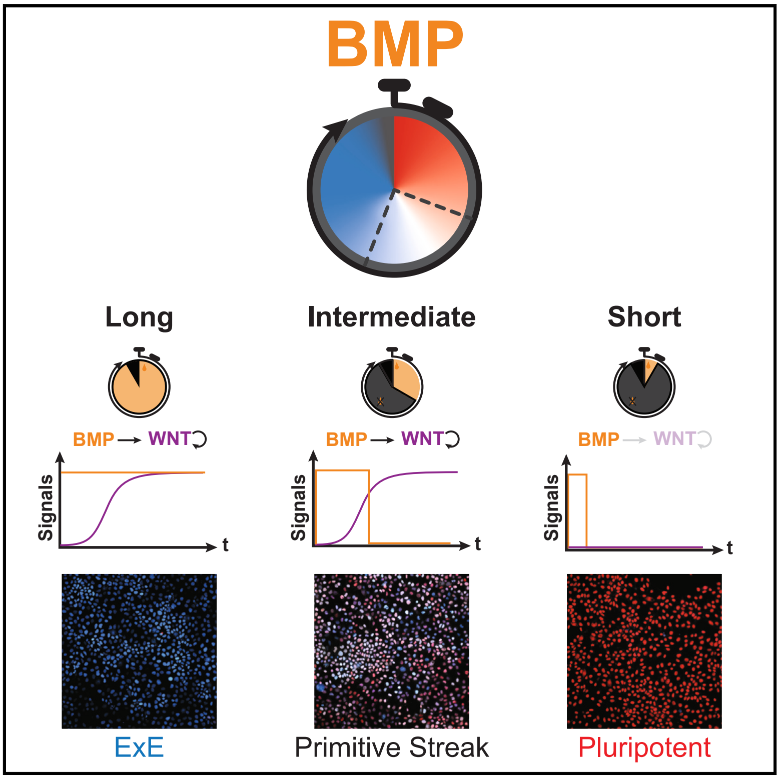

Highlights

- Investigated the effect of duration and concentration of BMP induction
- Intermediate and long high BMP pulses induce mesodermal and extraembryonic differentiation
- Constant low BMP does not effectively induce mesoderm differentiation at any dose
- Modeling shows how cell fate is a combinatorial response to BMP and endogenous WNT

Authors

Elena Camacho-Aguilar,
Sumin T. Yoon, Miguel A. Ortiz-Salazar,
Siqi Du, M. Cecilia Guerra,
Aryeh Warmflash

Correspondence

ecamagu@upo.es (E.C.-A.),
aryeh.warmflash@rice.edu (A.W.)

In brief

During embryonic development, cells are exposed to changing concentrations of morphogens over time. We investigated how cells interpret the duration and concentration of the gastrulation-inducing signal BMP4 and discovered that they are not interchangeable. We show how this is due to a combinatorial interpretation of BMP4 and endogenous Wnt.

Camacho-Aguilar et al., 2024, Cell Systems *15*, 445–461
May 15, 2024
https://doi.org/10.1016/j.cels.2024.04.001

Cell Systems

CellPress

Article

Combinatorial interpretation of BMP and WNT controls the decision between primitive streak and extraembryonic fates

Elena Camacho-Aguilar,[1,3,*] Sumin T. Yoon,[1] Miguel A. Ortiz-Salazar,[1] Siqi Du,[1] M. Cecilia Guerra,[1]
and Aryeh Warmflash[1,2,4,*]
[1]Department of Biosciences, Rice University, Houston, TX 77005, USA
[2]Department of Bioengineering, Rice University, Houston, TX 77005, USA
[3]Present address: Department of Gene Regulation and Morphogenesis, Andalusian Center for Developmental Biology (CSIC-UPO-JA), Seville 41013, Spain
[4]Lead contact
*Correspondence: ecamagu@upo.es (E.C.-A.), aryeh.warmflash@rice.edu (A.W.)
https://doi.org/10.1016/j.cels.2024.04.001

SUMMARY

BMP signaling is essential for mammalian gastrulation, as it initiates a cascade of signals that control self-organized patterning. As development is highly dynamic, it is crucial to understand how time-dependent combinatorial signaling affects cellular differentiation. Here, we show that BMP signaling duration is a crucial control parameter that determines cell fates upon the exit from pluripotency through its interplay with the induced secondary signal WNT. BMP signaling directly converts cells from pluripotent to extraembryonic fates while simultaneously upregulating Wnt signaling, which promotes primitive streak and mesodermal specification. Using live-cell imaging of signaling and cell fate reporters together with a simple mathematical model, we show that this circuit produces a temporal morphogen effect where, once BMP signal duration is above a threshold for differentiation, intermediate and long pulses of BMP signaling produce specification of mesoderm and extraembryonic fates, respectively. Our results provide a systems-level picture of how these signaling pathways control the landscape of early human development.

INTRODUCTION

In mammalian development, gastrulation is the first differentiation event of the embryo proper,[1,2] where the pluripotent epiblast differentiates into the three germ layers of the embryo: ectoderm, mesoderm, and endoderm. This process is orchestrated by a cascade of signals initiated by bone morphogenetic protein (BMP) signaling from the extraembryonic (ExE) tissues, which triggers Wnt and Nodal signaling in the epiblast.[3–5] The ligands for all three pathways find their highest expression in the proximal posterior portion of the embryo, where the primitive streak emerges, defining the anterior-posterior axis of the embryo.[6–8] However, how this cascade of signals combinatorially controls cell differentiation at this stage is still not completely understood.

Technical and ethical issues prevent the study of these questions *in vivo*, especially in the human embryo. To overcome this problem, several *in vitro* models of mammalian gastrulation have been developed that can serve as proxies for investigating these stages of development.[9–12] In particular, we and others have shown that human pluripotent stem cells (hPSCs) grown in colonies of precise size and shape using micropatterning technology and treated with the upstream gastrulation-inducing signal BMP4 pattern into all three germ layers plus a fourth one transcriptionally similar to extraembryonic tissues, which most likely represents the amnion.[13–20]

A classical framework for explaining how a signal can pattern a tissue is given by the French flag model.[21] In this model, the generation of a spatial signaling gradient (referred to as morphogen gradient in this context) is translated into a pattern by cells interpreting the level of morphogen concentration they are exposed to. However, several studies contradict the idea that BMP directly functions as a morphogen in a concentration-dependent manner in this system. First, in colonies of sizes of 10 cells or smaller, BMP acts as a switch controlling a cell state transition from pluripotency to extraembryonic as BMP concentration increases without inducing mesendodermal fates at any dose.[22] In fact, primitive streak induction only occurs when the cell density is above a threshold and is blocked if either the Wnt or Nodal pathways are inhibited.[14,22] Thus, secondary signals are necessary for BMP to induce differentiation into the three germ layers, and therefore BMP might not be acting as a classical morphogen in this context. However, much remains unknown about the underlying mechanisms.

Despite being intuitive, the French flag model also assumes that cells are exposed to a constant concentration of the morphogen in time. However, embryonic development is a highly dynamic process that involves rapid changes in the patterns of morphogen expression and large morphogenetic movements. Therefore, cells are exposed to changing concentrations of multiple morphogens over time. In fact, duration of signaling has been argued to play a key role not only in developmental patterning[23–30] but also in the response to stress and inflammatory signaling pathways, including nuclear factor κB (NF-κB)[31–34] and p53.[35] Still, the roles of concentration and duration of BMP signaling during human gastrulation and its interplay with other secondary signals to induce patterning remain an open question.

Here, we studied how cell fate decisions are controlled by BMP signaling during human pluripotent stem cell differentiation *in vitro*. We investigated how hPSCs interpret the duration and concentration of the applied BMP4 signal. Our results unveiled an apparent *morphogen effect* in time, where short, intermediate, and long pulses of BMP4 signaling result in cells either remaining pluripotent or differentiating to mesodermal or extraembryonic states, respectively. By contrast, varying the BMP concentration does not cause comparably efficient mesodermal differentiation at any dose. Using live-cell imaging of signaling and cell fate reporters together with mathematical modeling, we show that this effect is controlled by combinatorial interpretation of the exogenously supplied BMP4 and endogenously induced Wnt signaling. In particular, the temporal morphogen effect is due to the interplay of two features: the dynamics of BMP driving the conversion of pluripotent cells to extraembryonic fates and BMP upregulating secondary Wnt signaling, which in turn promotes mesoderm differentiation. Using a simple mathematical model, we uncovered the minimal requirements for the logic that controls these cell fate decisions, providing a fate map that explains how the BMP, WNT cascade governs early human developmental decisions. Our findings have implications for how signaling pathways control the landscape of early human development and highlight the importance of time in *in vitro* differentiation protocols.

RESULTS

BMP signaling produces a morphogen effect in time but not in concentration

As BMP induces extraembryonic fates directly but other fates through secondary signals,[3,22,36] we speculated that the timescales for these processes may differ, and the duration of BMP treatment may be an important variable. Previous differentiation protocols in hPSCs also indicated that the timing of BMP treatment may influence the outcome.[37] We cultured hPSCs for 2 days, exposing them to varying durations of BMP4 treatment of a fixed concentration, 10 ng/mL, at the outset (Figure 1A). We observed that cells that were exposed to a BMP pulse of 8 h or less remained in the pluripotent or undifferentiated state, as marked by high SOX2, OCT4, and NANOG expression (Figures 1B–1D, S1A, and S1B). On the other hand, BMP pulses longer than 32 h were necessary to differentiate cells uniformly into an extraembryonic state, marked by high CDX2, ISL1, HAND1, and GATA3 expression (Figures 1B–1D and S1C–S1F). Although the identity of these cells has been debated in the literature, transcriptome analysis has shown they are most similar to amnion, and, moreover, amnion differentiation has been shown to depend on BMP, while trophectoderm differentiation does not.[13,16,18–20] This is consistent with what is known about the lineages of these cell types in primate embryos *in vivo*, as only the amnion, but not the trophectoderm, derives from the epiblast.

Notably, pulses of 16 h showed a high level of mesoderm or primitive streak differentiation, marked by high T/BRACHYURY (BRA) expression (Figures 1B–1D). These results unveiled a morphogen effect in the duration of BMP signaling, with short, intermediate, and long pulses resulting in pluripotent, mesodermal, and extraembryonic fates, respectively. As ∼97% of the cells differentiate to an extraembryonic state if BMP is maintained for the entire 2 days protocol, this morphogen effect is not due to heterogeneity in the initial cell culture but to single cells interpreting the duration of the BMP signal to differentiate to either mesoderm or extraembryonic fates. That is, cells with the potential to adopt a mesodermal fate if the BMP is withdrawn differentiate to an extraembryonic fate with continued signaling.

Several studies have suggested that for other pathways, including Sonic Hedgehog, duration and amplitude of signaling may be interchangeable, with shorter treatment with higher doses being equivalent to longer exposure to low doses.[23,29] If this was the case for BMP signaling in hPSCs, the high proportion of mesodermal cells obtained with a pulse of intermediate duration should be reproduced by treating hPSCs with a constant 2 days pulse of a lower BMP concentration. To test this, we compared the results of treating cells with 10 ng/mL BMP4 pulses of intermediate durations (ranging from 14 to 24 h) (Figures 2A and 2B) to the results obtained by inducing hPSCs with several constant concentrations (ranging from 1 to 4 ng/mL) for 48 h (Figures 2C and 2D). We observed that constant induction by any lower BMP4 concentration could not reproduce the high percentage of mesoderm cells obtained with 10 ng/mL BMP4 for intermediate durations (Figures 2A–2D). Moreover, we obtained similar results when cells were maintained in constant BMP concentrations for 72 h. With longer BMP treatment, there was a shift toward extraembryonic fates from pluripotent ones, with this transition occurring at lower concentrations after 72 h of treatment compared with 48 h (Figures S2A and S2B). These results suggest that low constant BMP signaling induces slower differentiation but mainly to an extraembryonic fate. This is consistent with the idea that the exit from pluripotent is primarily responsive to the integral of BMP signaling (Teague et al.[38] and see below); however, it does not explain how the decision between primitive streak and extraembryonic fates is made and why it is sensitive to the duration of BMP.

To further investigate the interplay between concentration and time of exposure to control hPSC fate specification, we induced hPSCs with different pulses (increasing from 0 to 48 h in 6 h increments) of varying concentrations of BMP4 (ranging from 5 to 50 ng/mL) and assessed the cell fates after 48 h (Figures 2E–2G). We observed that when BMP4-containing media was withdrawn and replaced by fresh media, the data suggested that, for higher concentrations, shorter pulses were needed to induce mesoderm fates. Although this result might suggest a trade-off between time and concentration, an alternative possibility is that it could be due to only a partial shutdown of BMP signaling after higher doses of BMP are removed. This could result from higher doses being more difficult to completely remove compared with lower ones or from activation of endogenous BMP signals at higher doses.

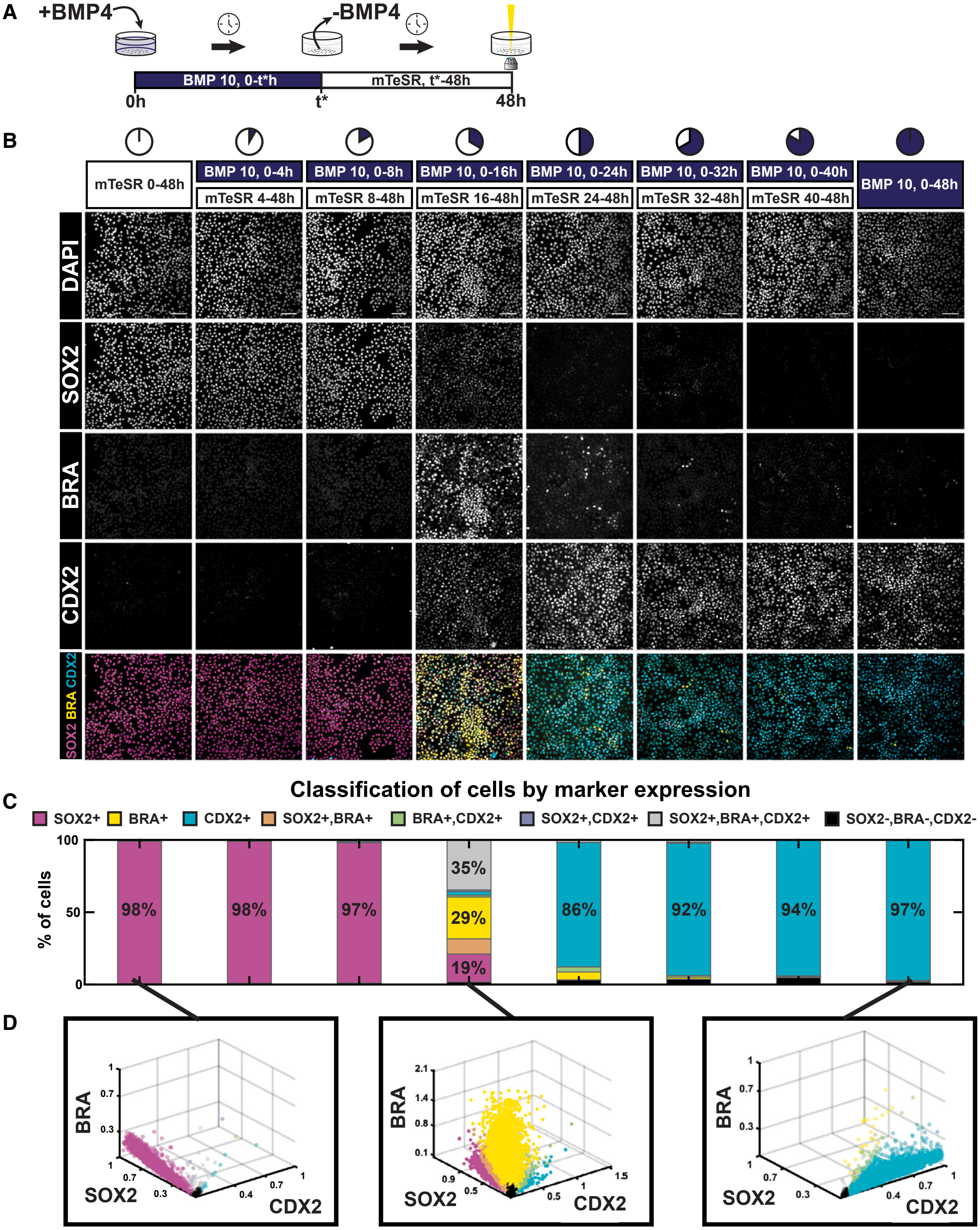

Figure 1. BMP4 signaling produces a morphogen effect in time

(A) Schematic of the induction protocol. hPSCs are treated with a pulse of 10 ng/mL BMP4 of varying durations (t*) after which the BMP-containing media is removed and replaced by the pluripotency maintenance media mTeSR1 (mTeSR). hPSCs are always fixed and immunostained 48 h after the onset of induction.

(B) Representative images of immunofluorescence for 4′,6-diamidino-2-phenylindole (DAPI), SOX2, BRA, and CDX2 after the indicated BMP4 treatments. Scale bars, 100 μm.

(C) Quantifications of cell fate proportions for the experimental conditions in (B). Regions in the SOX2, BRA, and CDX2 protein expression space where cells that exclusively express one of the markers are labeled with that marker “+,” while cells that express combinations of markers are labeled as mixed (see appendix for more details). *n* = 9 images per condition.

(D) From left to right, scatter plots of the quantifications of SOX2, BRA, and CDX2 for the conditions mTeSR 0–48 h, BMP 10 ng/mL 0–16 h followed by mTeSR 16–48 h, and BMP 10 ng/mL 0–48 h, respectively. Each dot corresponds to a single cell, and its color marks the cell fate assigned to the cell, as shown in (C).

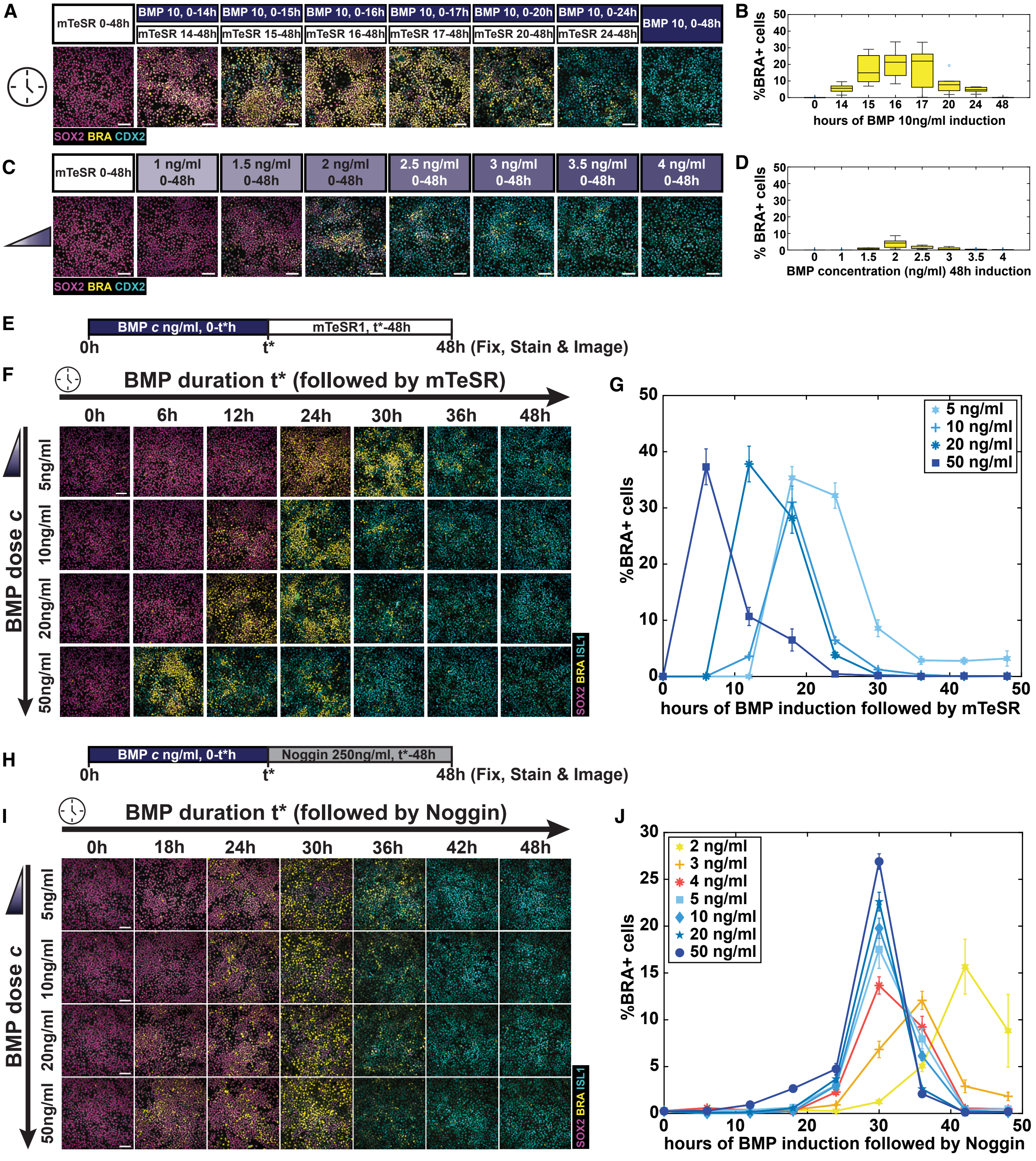

Figure 2. Duration and concentration of BMP4 signaling are not interchangeable

(A) Representative images of immunofluorescence for SOX2, BRA, and CDX2 in magenta, yellow, and cyan, respectively, after the indicated pulses of 10 ng/mL BMP4 treatments followed by mTeSR.

(B) Quantifications of the proportions of cells classified as BRA+ in the treatments shown in (A). *n* = 6 images per condition.

(C) Representative images of immunofluorescence for SOX2, BRA, and CDX2 in magenta, yellow, and cyan, respectively, after the treatments of the indicated constant concentrations of BMP4.

(D) Quantifications of the proportions of cells classified as BRA+ in the treatments shown in (C). *n* = 6 images per condition.

(legend continued on next page)

Therefore, we repeated the above experiment using a variety of different BMP durations and concentrations with a modified protocol in which BMP-containing media was replaced by media containing the BMP inhibitor Noggin (250 ng/mL) (Figure 2H). Mesoderm induction peaked with a BMP4 pulse of around 30 h for nearly all concentrations except for the lowest ones (Figure 2J). The later peak at lower concentrations is due to a slower induction of secondary signals necessary for mesoderm differentiation, as shown below (see Figures S4F and S4G). Notably, even though the most efficient duration of the BMP4 pulse was common for all concentrations above 3 ng/mL, quantification showed that higher concentrations yielded higher proportions of BRA-positive cells. Taken together, the results suggest that concentration and time of exposure are not interchangeable and that efficient mesoderm induction by 48 h of treatment required a pulse of a high BMP4 concentration for intermediate duration.

BMP signal induces WNT in a bistable fashion

To understand how signaling dynamics underlie our results on cell fate induction, we took advantage of live-cell reporters of signaling activity to measure the signaling response in time under different treatment conditions. In particular, we first tracked the BMP4 response by performing live imaging of hPSCs with a GFP::SMAD4 fusion in the endogenous locus[22] and quantified the strength of the signaling response as the ratio of nuclear and cytoplasmic SMAD4 intensity (Figures 3A–3D and S3). Consistent with our previous work,[22,39] a sudden increase in BMP4 leads to a rapid translocation of SMAD4 into the nucleus in less than 30 min. This response was sustained with a gradual decrease in activity over time for the remaining 48 h if BMP4 was kept in the media (Figures 3D and S3). The addition of Noggin resulted in a rapid decrease in nuclear SMAD4 to baseline (Figures 3D and S3A). Consistent with our previous observations, removal of BMP4 without Noggin addition resulted in a rapid reduction in nuclear SMAD4 but to a higher level than baseline, indicating that either some exogenous BMP4 remains in the media or endogenous BMPs remain active once the exogenous signals are removed (Figures 3D and S3A). As the SMAD4 cofactor also translocates to the nucleus in the presence of Nodal signaling, we repeated the experiment, this time also adding the Activin/Nodal inhibitor SB431542 throughout (Figure S3C). The observed SMAD4 dynamics were identical with or without the Activin/Nodal inhibitor SB431542, suggesting that there were no important endogenous Nodal levels in the media and that SMAD4 reflected the response to BMP4 treatment exclusively.

We then explored WNT/β-catenin response, the next member of the signaling cascade that plays a role in gastrulation and mesoderm differentiation.[1] We tracked WNT response by performing live imaging of hPSCs with GFP fused to the N terminus of endogenous β-catenin[40] and quantified the strength of the signaling response as the mean nuclear β-catenin intensity (Figures 3E–3H). Notably, measurement of Wnt dynamics revealed a bistable WNT/β-catenin response (Figures 3H, S4A, and S4C). If BMP was withdrawn early, β-catenin levels converged to a low level over time. However, if BMP was presented for sufficiently long, WNT activity became self-sustaining and remained stable even after BMP withdrawal. It is important to note that the differences between conditions in the levels of β-catenin activation were not due to averaging over cells in low and high states as, even though there was heterogeneity between cells, the distributions of β-catenin levels observed were monomodal for all conditions (Figure S4E). In particular, all conditions had a Sarle's bimodality coefficient lower than 5/9 for all times and no heavy tails, as the differences between the mode and the mean of the distributions were low.

We then checked whether the observed WNT self-sustaining response was due to positive feedback in which WNT activates its own ligands, as shown in other contexts.[41] We performed bulk RNA sequencing of cells exposed to either 300 ng/mL of the ligand WNT3A for 6 or 18 h, or 8 mM of the GSK3β inhibitor CHIR99021 for 6 h, which is commonly used as a substitute for WNT in differentiation protocols (Figures 3I and S5A). We observed transcriptional activation of the canonical WNT genes *WNT3* and *WNT10B* (Figures 3I and S5A), confirming that Wnt signaling induces canonical WNTs. Moreover, we compared WNT/β-catenin response in the presence and absence of the WNT ligand secretion inhibitor IWP2 under WNT3A treatment (Figure S5B). In both cases, we observed an adaptive response as described in Massey et al.[40] However, the response with IWP2 treatment adapted to a significantly lower level, converging to a basal level over time (Figure S5B), suggesting that the canonical WNT ligands induced downstream of exogenous treatment are secreted and function to further elevate signaling levels. Finally, to further confirm that the sustained endogenous WNT/β-catenin response induced under a BMP pulse was due to the activation of endogenous WNT ligands, we treated cells with a BMP pulse followed by Noggin and compared the WNT/β-catenin response to that obtained when IWP2 was also added together with Noggin (Figure S5C). Adding Noggin+IWP2 notably reduced WNT/β-catenin response in comparison with just

(E) Schematic of the induction protocol performed in (F). hPSCs are treated with a pulse of different BMP4 concentrations (c) of varying durations (t*), after which the BMP-containing media is removed and replaced by the pluripotency maintenance media mTeSR1 for the remainder of the 48 h protocol (i.e., 48-t* h).

(F) Representative images of immunofluorescence for SOX2, BRA, and CDX2 in magenta, yellow, and cyan, respectively, after the 48 h treatments with pulses of the indicated times (columns) followed by mTeSR, of the indicated concentrations (rows) of BMP.

(G) Quantifications of the proportions of cells classified as BRA+ in the treatments shown in (E). *n* = 6 images per condition.

(H) Schematic of the induction protocol performed in (I). hPSCs are treated with a pulse of different BMP4 concentrations (c) of varying durations (t*), after which the BMP-containing media is removed and replaced by media containing Noggin (250 ng/mL) for the remainder of the 48 h protocol (i.e., 48-t* h).

(I) Representative images of immunofluorescence for SOX2, BRA, and CDX2 in magenta, yellow, and cyan, respectively, after the 48 h treatments with pulses of the indicated times (columns) followed by Noggin, of the indicated concentrations (rows) of BMP.

(J) Quantifications of the proportions of cells classified as BRA+ after 48 h of treatment with pulses of the indicated concentrations (legend) and indicated time lengths (x axis) followed by Noggin treatment. *n* = 8 images per condition. Error bars in (G) and (J) show the SEM.

Error bars indicate standard error of the mean (SEM). Boxplots show the median, the lower and upper quartiles, the minimum and maximum values that are not outliers within the whiskers, and any outliers (computed using the interquartile range) as dots. Scale bars, 100 μm.

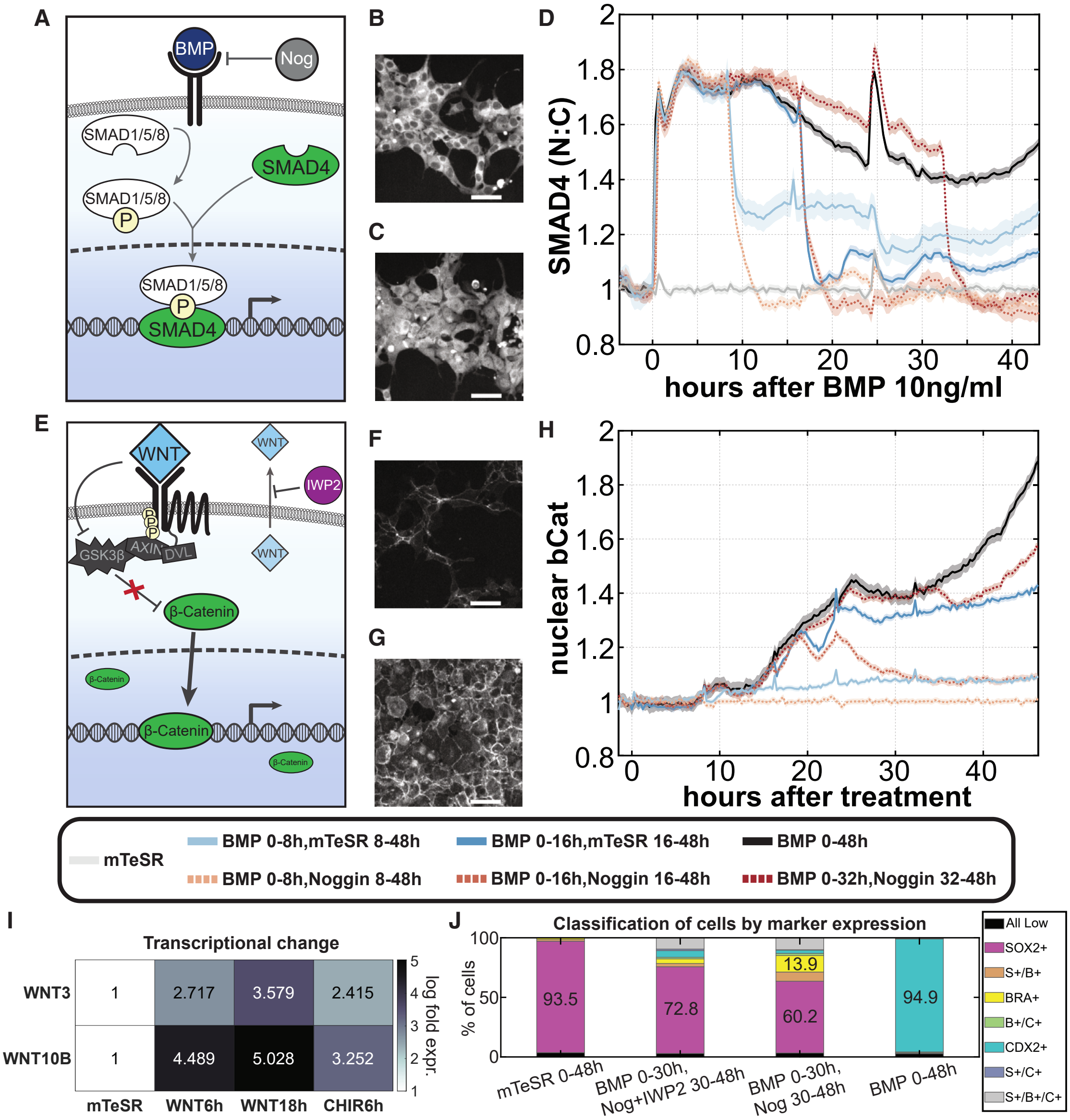

Figure 3. BMP signaling induces a bistable endogenous WNT

(A) BMP signal is transduced through SMAD4 translocation to the nucleus. Noggin inhibits BMP signal by preventing it from binding to the receptors.

(B and C) Representative images of hPSCs expressing GFP::SMAD4 before BMP4 10 ng/mL treatment (B) and 5 h after treatment with BMP4 10 ng/mL (C).

(D) GFP::SMAD4 average nuclear:cytoplasmic intensity ratio after the treatments with 10 ng/mL of BMP indicated at the bottom of the figure. The standard error is shown as a shaded contour. Additional experimental conditions are shown in Figure S3A. *n* = 8 movies per condition.

(E) Simplified canonical WNT/β-catenin pathway. IWP2 prevents canonical WNT secretion.

(F and G) Representative images of hPSCs expressing GFP::β-catenin before BMP 10 ng/mL treatment (F) and 40 h after treatment with BMP4 10 ng/mL (G).

(H) GFP::β-catenin average nuclear intensity after the treatments with 10 ng/mL of BMP indicated at the bottom of the figure. Data were normalized to the BMP 0–8, Noggin 8–48 h condition, as it showed similar dynamics to the mTeSR condition (Figure S3C). The standard error is shown as a shaded contour. Additional experimental conditions are shown in Figures S3B and S3C. *n* = 8 movies per condition.

(I) Normalized gene counts for upregulated canonical WNT ligands under the indicated treatments. Averaged over *n* = 2 biological repeats.

(J) Quantifications of cell fate proportions for the indicated treatment. The concentration of BMP used was 10 ng/mL, followed by Noggin, with or without IWP2. *n* = 5 images per condition. Scale bars, 50 μm.

adding Noggin (Figure S5C), which indicates that a WNT positive feedback loop is responsible for elevating signaling levels beyond those that result from the WNT levels induced by BMP alone. Taken together, these results suggest that WNT/β-catenin response becomes self-sustained after a sufficiently long BMP4 pulse due to induction of expression and secretion of canonical WNT ligands.

Comparing the signaling trajectories with the resulting fates reveals that only in cases where BMP is repressed after having induced WNT to a high level are cells able to differentiate to

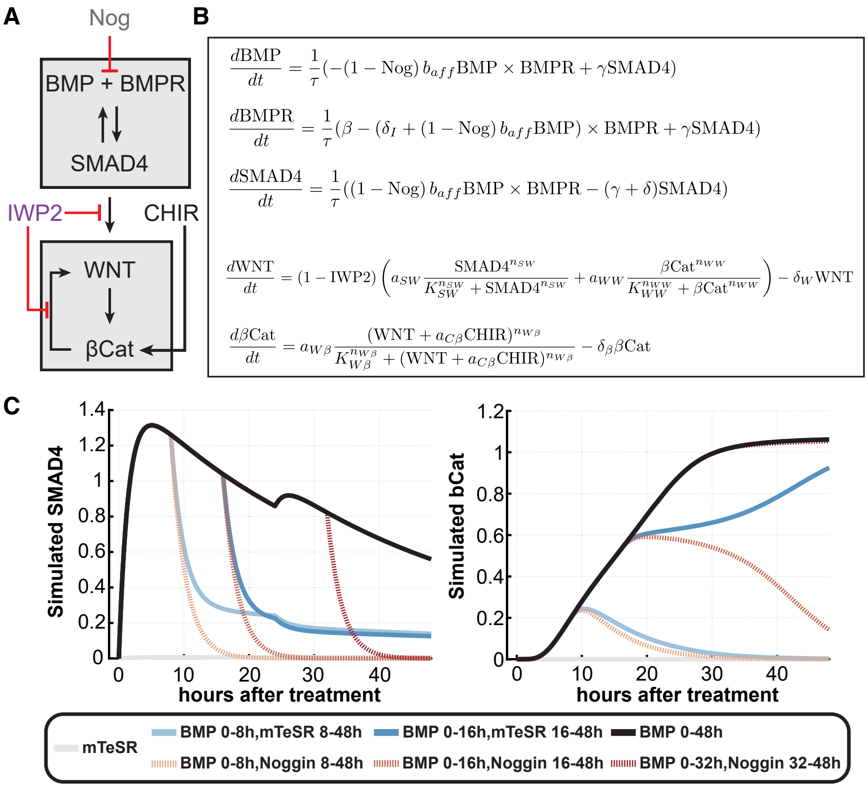

$$\frac{d\mathrm{BMP}}{dt} = \frac{1}{\tau}(-(1-\mathrm{Nog})\,b_{aff}\mathrm{BMP}\times\mathrm{BMPR}+\gamma\mathrm{SMAD4})$$

$$\frac{d\mathrm{BMPR}}{dt} = \frac{1}{\tau}(\beta-(\delta_I+(1-\mathrm{Nog})\,b_{aff}\mathrm{BMP})\times\mathrm{BMPR}+\gamma\mathrm{SMAD4})$$

$$\frac{d\mathrm{SMAD4}}{dt} = \frac{1}{\tau}((1-\mathrm{Nog})\,b_{aff}\mathrm{BMP}\times\mathrm{BMPR}-(\gamma+\delta)\mathrm{SMAD4})$$

$$\frac{d\mathrm{WNT}}{dt} = (1-\mathrm{IWP2})\left(a_{SW}\frac{\mathrm{SMAD4}^{n_{SW}}}{K_{SW}^{n_{SW}}+\mathrm{SMAD4}^{n_{SW}}}+a_{WW}\frac{\beta\mathrm{Cat}^{n_{WW}}}{K_{WW}^{n_{WW}}+\beta\mathrm{Cat}^{n_{WW}}}\right)-\delta_W\mathrm{WNT}$$

$$\frac{d\beta\mathrm{Cat}}{dt} = a_{W\beta}\frac{(\mathrm{WNT}+a_{C\beta}\mathrm{CHIR})^{n_{W\beta}}}{K_{W\beta}^{n_{W\beta}}+(\mathrm{WNT}+a_{C\beta}\mathrm{CHIR})^{n_{W\beta}}}-\delta_\beta\beta\mathrm{Cat}$$

Figure 4. BMP-induced WNT bistability is reproduced by a simple mathematical model

(A) Schematic of the network regulating BMP and WNT response.

(B) System of ordinary differentiation equations (ODEs) that model the network dynamics in (A).

(C) Simulations of BMP and WNT dynamics under the indicated BMP4 treatments. Media change is also simulated at 24 h for all conditions. BMP, BMP4 ligand; BMPR, BMP4 receptors; SMAD4, nuclear SMAD4; Nog, Noggin; WNT, WNT ligands; βCat, nuclear β-catenin; CHIR, CHIR99021.

mesoderm. This suggests that a combinatorial effect between BMP and BMP-induced bistable Wnt signals underlies the observed morphogen effect in time. Short BMP durations of high BMP concentration are too transient to activate WNT, and, therefore, cells remain pluripotent. On the other hand, if BMP is maintained for longer than 32 h, Wnt signaling is induced but is insufficient to override the effects of BMP signaling, and cells become extraembryonic. It is in a window of middle durations, where BMP is maintained for long enough to induce Wnt autoactivation but is then suppressed, that cells are exposed to a low BMP, high Wnt signaling profile for a sufficient window of time, and mesoderm differentiation is obtained. Moreover, we observe that the rate of increase of nuclear β-catenin increased as the BMP dose increased (Figure S4F), and this was also reflected in the dynamics of WNT target genes as LEF1 and BRA (Figure S4G). This explains why low concentrations are not as efficient at inducing mesoderm, as a constant low concentration of BMP4 is slow at upregulating Wnt signaling and downstream targets.

In order to explicitly confirm that mesoderm differentiation is dependent on WNT/β-catenin response, we investigated the effect of adding IWP2 after BMP4 withdrawal, both with and without Noggin (Figures 3J, S5D, and S5E). As expected, the addition of IWP2 in the washing media significantly reduced or even prevented mesoderm induction (Figures 3J, S5D, and S5E). We also investigated how WNT/β-catenin response depended on cell density, as previous studies have shown that cell density is critical for BMP signal to induce mesodermal fates.[22] Consistent with these studies, we observed that if we reduced the number of cells seeded from 40,000 cells/cm^2 to 15,000 cells/cm^2, pulses of BMP of high concentration could no longer induce mesoderm (Figures S6A–S6D). To understand whether the lack of mesoderm correlated with reduced WNT signaling, we compared the WNT response of cells seeded at a density of 40,000 cells/cm^2 (high density) versus cells seeded at a density of 15,000 cells/cm^2 (low density) by performing live imaging of the β-catenin reporter cells (Figure S6E). Indeed, we observed that the WNT response under BMP treatment was lower at low densities. Although BMP induced a high WNT response in cells seeded at high density, the WNT response of cells seeded at low density under the same BMP treatment was comparable to non-treated cells at high density (Figure S6E).

Taken together, these results suggest that BMP induces a bistable endogenous WNT signal in a concentration-dependent manner, which is necessary for mesoderm induction. The mechanism behind this process will be discussed further below.

A simple mathematical model reproduces the observed WNT bistability

To better understand the observed WNT bistability, we developed a minimal mathematical model that recapitulated the signaling dynamics described above. This model comprises two subsystems of differential equations that model the BMP and Wnt responses, respectively, and which are connected via BMP4 activation of Wnt, reflecting the transcriptional activation of *WNT3* by BMP signaling (Figures 4A and 4B).[42] For simplicity, and since we do not observe multi-modality in the response to signals in time, the model aims to reflect the average response to the signals in time within the cell population. Moreover, our goal is to model the signaling response observed when cells are grown in high density (40,000 cells/cm^2), as otherwise, Wnt signaling is not present.

We simulated the BMP response using the model proposed in Heemskerk et al.,[39] where the binding of BMP ligands to the receptor complex activates SMAD4 but enhances the degradation of the BMP receptor (Figures 4A and 4B). The effect of the BMP inhibitor Noggin is modeled by a direct inhibition of BMP binding to free receptors (Figures 4A and 4B). For simplicity, BMP withdrawal without Noggin addition was modeled by multiplying the

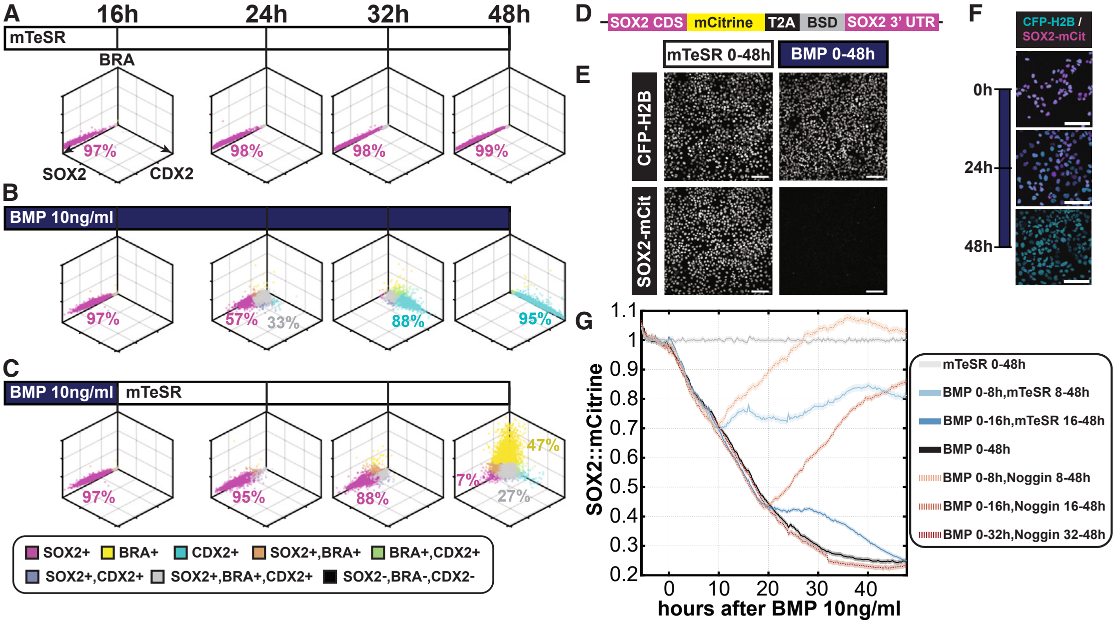

Figure 5. Cell fate transitions under BMP treatment

(A–C) Scatter plots of the quantifications of SOX2, BRA, and CDX2 under the treatments mTeSR 0–48 h (A), BMP 10 ng/mL 0–48 h (B), and BMP 10 ng/mL 0–16 h followed by mTeSR 16–48 h (C), at 16, 24, 32, and 48 h. Each dot corresponds to a single cell, and its color marks the cell fate assigned to the cell as shown in the legend at the bottom.

(D) Schematic of resulting mRNA transcribed from the labeled SOX2 allele after CRISPR-Cas-mediated SOX2-mCitrine-T2A-BSD knockin. The blasticidin resistance protein (BSD) facilitates the selection of labeled cells. T2A is a self-cleaving peptide that enables the separation of BSD from SOX2::mCitrine.

(E) Representative images of hPSCs with mCitrine-labeled SOX2 and the nuclear marker CFP::H2B. (Left) Under no treatment. (Right) SOX2 expression is lost after 48 h of 10 ng/mL BMP4 treatment.

(F) Representative confocal microscopy images of live SOX2::mCitrine hPSCs at 0, 24, and 48 h after treatment with 10 ng/mL BMP4.

(G) SOX2::mCitrine average nuclear intensity after the indicated treatments. *n* = 8 movies per condition. The standard error of the mean (SEM) is shown as a shaded contour. Scale bars, 100 μm.

original BMP concentration by a constant representing the percentage of BMP that remained in the culture, as observed in Figures 3D, S3A, and S3C. This model was able to reproduce features of SMAD4 dynamics observed in the data, such as fast SMAD4 upregulation upon BMP4 treatment, rapid SMAD4 downregulation by Noggin, and slow decay (Figures 4C, S7A, and S7B).

The second sub-system models the Wnt response. In this model, Wnt expression is activated by SMAD4 and activates nuclear β-catenin. β-catenin, in turn, further activates Wnt signaling. The need to accumulate sufficient Wnt protein before b-catenin becomes active explains the delay in the rise in β-catenin activity observed experimentally (see Figure 3H). Details of this model can be found in the appendix in supplemental information.

The model composed of the two subsystems could reproduce the observed BMP-induced WNT bistability (Figures 4C and S7; see appendix in supplemental information). Short BMP pulses allowed the β-catenin variable to remain in a low steady state, while longer BMP pulses resulted in the β-catenin variable converging to a high steady state where it remained even in the absence of BMP (Figure 4C). The model also reproduced the signaling dynamics obtained under BMP withdrawal without Noggin and the BMP concentration-dependent increase of WNT signaling (Figure S7). Notably, as in the experimental data, while a 16 h pulse of BMP followed by Noggin inhibition resulted in β-catenin returning to a low value, a 16 h pulse of BMP followed by withdrawal without Noggin resulted in β-catenin auto-activating to a high level by 48 h (Figures S3A–S3C, S7A, and S7C). Thus, modeling supports the idea that residual BMP in the media explains why a 16 h pulse of BMP 10 ng/mL is sufficient to induce mesoderm if the BMP-containing media is replaced by media alone, while longer pulses are needed if Noggin is used.

Mesoderm induction correlates with a slow loss of pluripotency

Our next goal was to understand the dynamics of the cell fate transitions. We treated hPSCs with pulses of 10 ng/mL BMP of varying durations and examined marker gene expression at 16, 24, 32, and 48 h after treatment (Figures 5A–5C and S8). As expected, when cells were not exposed to BMP, they remained pluripotent, as marked by high SOX2 expression at every time point observed (Figure 5A). On the other hand, if hPSCs were exposed to BMP for the entire 48 h, a pluripotent-to-extraembryonic transition was observed between 24 and 32 h, when cells downregulated SOX2 and then upregulated CDX2 (Figure 5B). It is important to note that, although cells transitioned through a transient state (state marked as (SOX2+, BRA+, CDX2+) in figures) at 24 h, where they expressed lower levels of SOX2 and slightly higher levels of BRA and CDX2 compared with the pluripotent state, the expression of BRA and CDX2 laid in the lower end of the range of expression of these genes in differentiated mesoderm (BRA+) or extraembryonic (CDX2+) cells. These results indicate that, under continuous BMP treatment, cells transition directly to extraembryonic without differentiating to a mesoderm state first. Finally, in the experimental conditions where mesoderm differentiation was obtained, such as 16 h of 10 ng/mL BMP4 followed by mTeSR, a slow SOX2 downregulation was observed, followed by a late BRA upregulation, starting after 32 h of induction (Figure 5C). This late mesoderm induction is consistent with recent studies that propose that SOX2 levels need to be low for Wnt to induce mesoderm differentiation.[43]

To observe gene expression dynamics with a higher time resolution, we used CRISPR-Cas9 genome engineering to insert mCitrine at the endogenous locus to form a C-terminal fusion with SOX2 (SOX2::mCitrine) (Figures 5D and S9; STAR Methods). To facilitate nuclear identification and analysis, the cells also express CFP::H2B, which was incorporated into the genome using the ePiggyBac transposable element system.[44] Treatment of these cells with BMP4 showed a rapid downregulation of SOX2, with undetectable expression after 2 days of treatment (Figures 5E, 5F, S9A, and S9B), and antibody staining for SOX2 and other pluripotency markers showed that these cells shared similar behavior to wild-type (WT) hPSCs (Figures S9C–S9H).

We imaged SOX2::mCitrine cells under different BMP4 treatments and observed the SOX2 dynamics for 2 days. Consistent with the results above, SOX2 expression was maintained in cells that were not exposed to BMP4 (Figure 5G). On the other hand, SOX2 expression rapidly began to decay under BMP4 treatment as soon as 3 h after treatment, and with a rate that was initially proportional to BMP4 concentration (Figures 5G and S9D). If BMP4 was withdrawn from the media early enough, SOX2 expression returned to high levels, while if cells were induced with long pulses of BMP4, they lost SOX2 expression. Notably, with a 16 h pulse of 10 ng/mL BMP4, which leads to peak mesoderm differentiation, SOX2 downregulation slowed after 16 h. A second phase of SOX2 decay led to hPSCs eventually losing SOX2 expression but later than cells induced under longer BMP4 pulses (Figure 5G). These results show that mesoderm induction correlates with a slow SOX2 decay after BMP withdrawal.

The initial decay of SOX2 expression is strongly correlated with the integral of the SMAD4 response to BMP4 in time (Figures S10A–S10E), suggesting that there is a trade-off between the magnitude and the duration of signaling in the dissolution of the pluripotent state. This correlation no longer holds in later times (Figure S10E), and the total integral of the BMP4 signal does not directly translate to cell fate (Figure S10F). This supports the hypothesis that the integral of BMP activity initially controls the exit from pluripotency, and the combinatorial interpretation of BMP and endogenous WNT signaling controls the decision between ExE and mesoderm fates.

In summary, these results suggest that BMP4 concentration initially regulates SOX2 expression, which rapidly starts to decay after BMP4 treatment at a rate that is proportional to SMAD4 activity. If BMP4 is removed early, SOX2 expression recovers to baseline, and cells remain pluripotent. Long BMP4 treatments produce a direct pluripotency-to-ExE transition without going through an intermediate mesoderm state. On the other hand, treatments with an intermediate BMP4 pulse produce a two-phased SOX2 downregulation, with an initial fast partial decay followed by a slow decay to baseline, which correlates with the onset of mesoderm induction.

A simple network model can recapitulate the observed dynamics

To understand how signal dynamics controlled the observed cell fate transitions, we aimed to create a mathematical model that recapitulated the experimental data. Numerous studies have shown that mathematical modeling either of the underlying gene regulatory network[45–48] or a recent approach focusing on the higher-level Waddington landscape[49–56] can provide information about the logic that controls cell state transitions. Due to the nature of our data, we aimed to create an intermediate mathematical model that contained some mechanistic information about the regulatory dynamics, allowing us to leverage the gene expression dynamics data while being simple enough to intuitively explain the cell state transitions that controlled the underlying differentiation process. With this in mind, we created a minimal cell fate network (CFN) model, where the nodes of the network correspond to the cell fates observed, i.e., pluripotent, mesodermal, and extraembryonic, characterized by high SOX2, BRA, or CDX2 expression, respectively, and coupled this CFN model with the signaling model described above (Figure 6A). For simplicity, we modeled SOX2, BRA, and CDX2 expression in time as a proxy for the corresponding cell fates. It is important to note, as mentioned above, that although we justify the construction of the CFN model below, the CFN does not aim to model all mechanistic interactions between particular genes, and therefore, direct links in the network should not be taken literally. Instead, our aim is to model the underlying logic by which cells transition between different cell fates with a simple network model for which we could leverage the gene expression dynamics data.

First, to generate mutually exclusive cell states, we included mutually repressive interactions between the pluripotency, mesoderm, and extraembryonic nodes of the network (Figure 6A). Secondly, as previous studies have shown and our data support that BMP activation of SMAD complexes leads to transcription of ExE markers such as GATA3, CDX2, and ISL1,[13,16,57–59] we included activation of CDX2 expression, and therefore induction of the ExE state, by nuclear SMAD4 through a Hill equation (Figure 6A; see appendix in supplemental information). We also observed that once the expression levels of ExE markers such as CDX2 and ISL1 became high, they remained high even if BMP was withdrawn from the media, suggesting a possible autoregulation of ExE markers, which we modeled by an additive autoactivation (Figure 6A; see appendix in supplemental information).

As WNT signals are necessary for BMP-induced mesoderm formation, as shown in Figures 3J, S5D, and S5E, and previous literature,[14,22,36] we considered that mesoderm markers are upregulated through β-catenin activation by WNT and modeled the activation of BRA expression through a Hill function of β-catenin levels (Figure 6A; see appendix in supplemental information).

Moreover, the SOX2 expression dynamics observed in Figure 5G suggested a downregulation of SOX2 by BMP. We

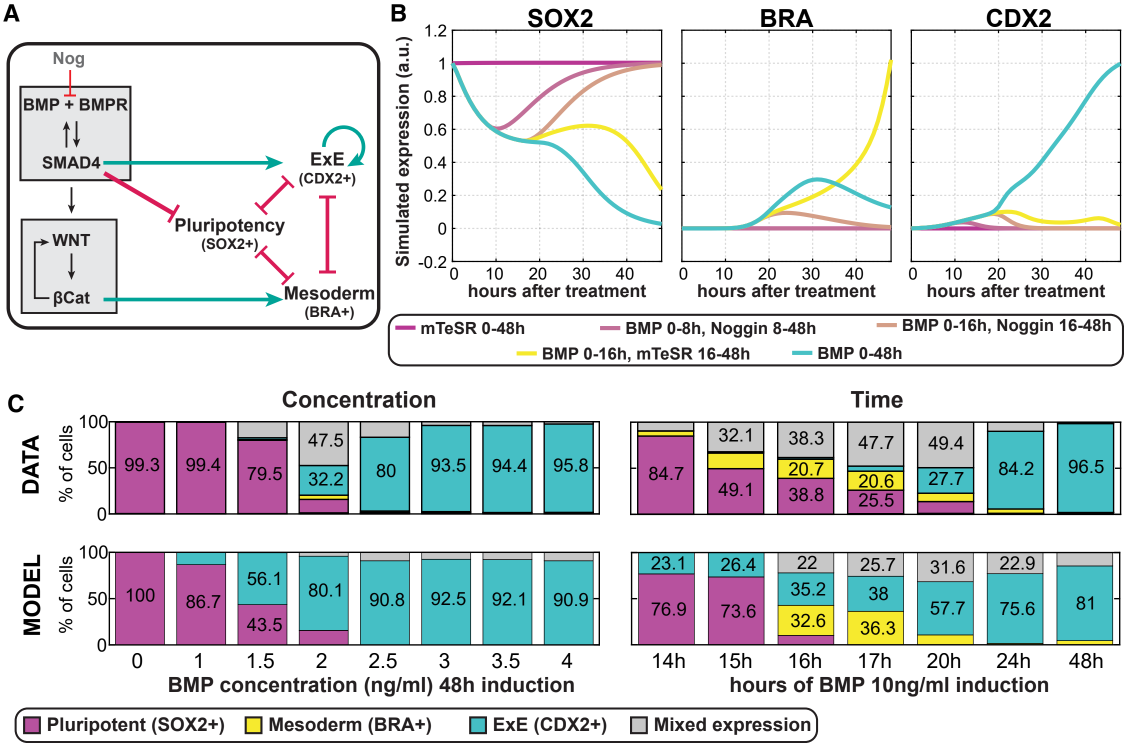

Figure 6. A minimal cell fate network can recapitulate the observed dynamics

(A) Schematics of the coupling of the signaling network and the minimal cell fate network.

(B) Simulated SOX2, BRA, and CDX2 dynamics from the model in (A) for the indicated experimental conditions.

(C) Experimental (top) and simulated (bottom) cell fate proportions under constant low concentrations (left) and pulses of BMP 10 ng/mL (right).

observe that SOX2 expression begins to decay rapidly upon BMP treatment (as early as 3 h). At this stage, neither Wnt signaling, as reflected in nuclear β-catenin, nor mesoderm or ExE markers are yet upregulated (Figures 3H and 5A–5C). Moreover, as mentioned above, our data show that the initial rate of SOX2 decay strongly correlated with SMAD4 levels for different concentrations and durations (Figure S10). Although we do not rule out the idea that this inhibition might be through an intermediate BMP target such as GATA3, which shows a similarly fast upregulation upon BMP treatment (Figure S10G), for simplicity, we modeled a direct inhibition of SOX2 expression levels by SMAD4 (Figure 6A; see appendix in supplemental information).

This minimal deterministic CFN model was fitted to simplified expression levels obtained in a subset of experiments using a Monte Carlo optimization algorithm, the details of which can be found in the appendix in supplemental information. The final fitted model was compatible with the dynamics observed in the data, such as direct pluripotency-to-ExE transition without expressing BRA under constant 2 days BMP4 induction. The model was also able to mimic the slow SOX2 decay under an intermediate pulse of BMP4, which also resulted in a late BRA upregulation (Figure 6B). Notably, the model was able to reproduce features and conditions that were not used in the fitting, such as the observed SOX2 dynamics for different BMP4 concentrations, and that a longer pulse of 5 ng/mL BMP is necessary for cells to differentiate to ExE compared with 10 ng/mL BMP when replaced by mTeSR following BMP withdrawal (Figure S11).

Having fitted the deterministic CFN model to the available data, we generated a stochastic version by considering an additive white noise of strength x to test whether the model could reproduce the cell fate proportions observed in the data. We fixed all the parameters from the deterministic model and fitted only the single noise parameter and the initial distribution of SOX2 expression to the cell fate proportions obtained in a subset of experimental data (see appendix in supplemental information). We found that, without modification to any of the parameters from the deterministic model, the stochastic model reproduced the observed BMP morphogen effect in time and the low mesoderm induction at any low constant concentration (Figure 6C). Taken together, the simple CFN model recapitulated the dynamics and cell proportions observed in the data, including in a large amount of data not used to fit the model parameters.

Cell fate is a combinatorial response to BMP and WNT

With the resulting model, we then aimed to understand how the signals BMP and WNT controlled cell fate determination. We created a phase diagram, or fate map, that shows, for a given value of SMAD4 and β-catenin, which cell fates are stable, or, in other words, accessible, in the deterministic model under those signaling levels (Figure 7A). For example, for low SMAD4 and β-catenin levels, only the pluripotent (P; SOX2+)

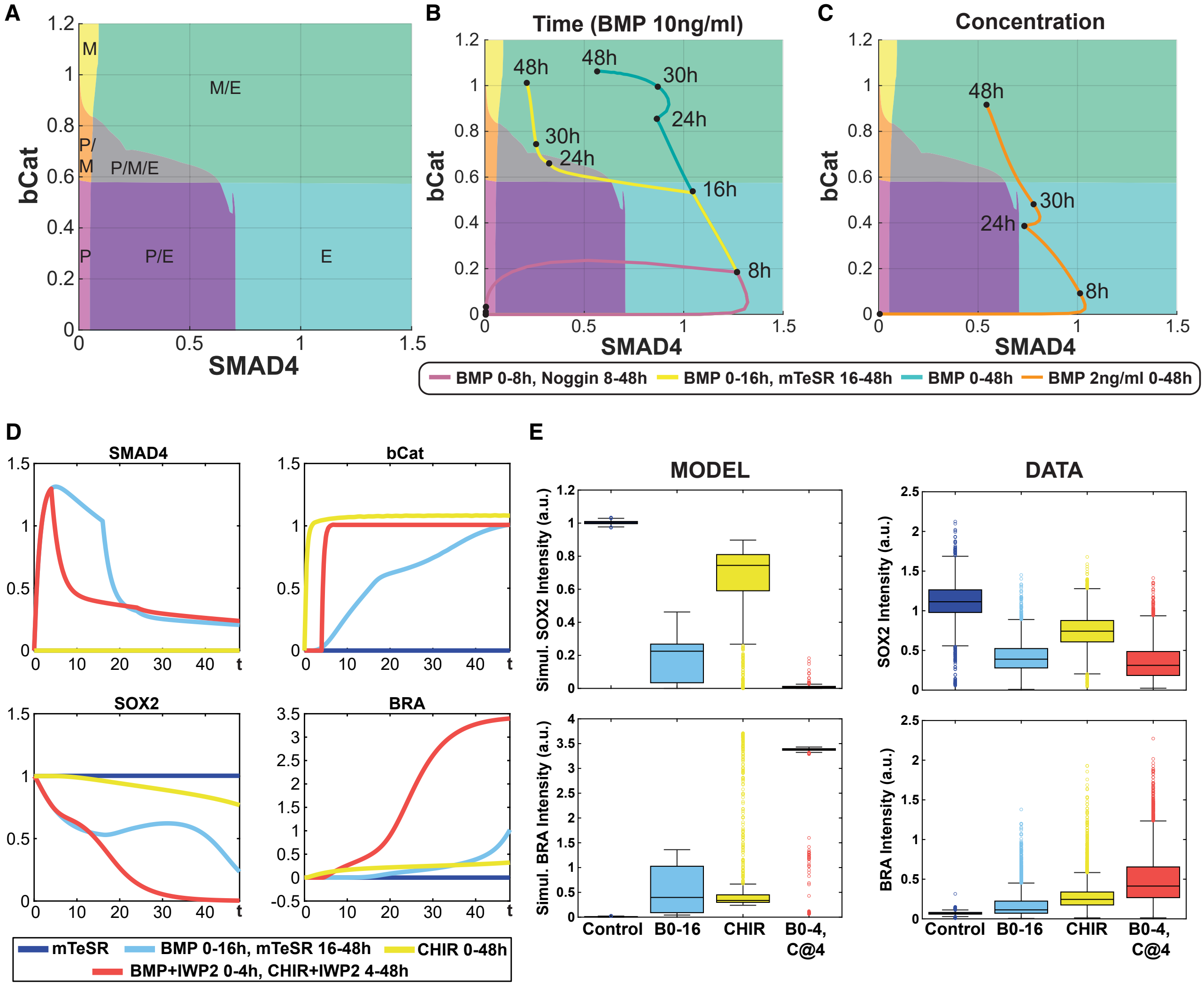

Figure 7. Cell fate is a combinatorial response to BMP and WNT

(A) Fate map defined by BMP (SMAD4) and WNT (bCat) levels obtained from the model in Figure 6. P, pluripotency; M, mesoderm; and E, extraembryonic.

(B) Signaling trajectories on the fate map for the indicated BMP10 ng/mL pulses.

(C) Signaling trajectory on the fate map for constant 2 ng/mL BMP4 induction.

(D) Simulated SMAD4, β-catenin, SOX2, and BRA dynamics for the conditions indicated on the legend.

(E) Predicted (top) cell proportions and their corresponding experimental confirmation (bottom).

state is stable, and therefore, cells remain pluripotent under low BMP and WNT levels. On the other hand, for high SMAD4 values and low β-catenin levels, the only stable state is the ExE (E; CDX2+) fate; therefore, the model suggests that cells would eventually adopt the ExE fate if induced with high BMP while inhibiting WNT signaling. For high SMAD4 and high β-catenin levels, a bistable region is defined, where both the mesodermal (M; BRA+) and ExE fates are accessible, and cells will become one or the other depending on the initial state of the cell.

However, cells are normally not exposed to constant SMAD4 and β-catenin levels, but they experience the signaling dynamics discussed previously, some of which are measured in Figure 3. Combining these signaling trajectories and the fate map, the model explains the experimental observations by showing that cell fate is a combinatorial response to BMP and WNT. Under short pulses of BMP, endogenous WNT is not activated, so the signaling trajectory moves to a high BMP region for a short period of time, after which it goes back to a low BMP, low WNT profile, and cells stay pluripotent (Figures 7B, pink curve, and S12). Under constant high BMP, endogenous WNT is activated, and the signal trajectory ends up in a region of high BMP and high WNT, where both ExE and mesoderm differentiation are possible. However, the cell trajectory lies in the basin of attraction of the ExE fate, and therefore cells adopt this fate (Figure 7B, blue curve). Under medium durations where WNT becomes self-sustained, even though the signal trajectory initially moves in a high BMP region for some time, during which the SOX2 levels in the cell decrease, the withdrawal of the BMP signal situates the signal trajectory in a region of tristability where all three fates are stable (Figures 7A and 7B, gray region), which slows down the decay of pluripotent markers and prevents cells from increasing the expression of ExE markers (Figures 7B, yellow curve, and S12A–S12C). This allows cells to become mesoderm once WNT increases and the signaling trajectory moves to the bistable ExE and mesoderm region (Figures 7B, yellow curve, and S12A–S12C). On the other hand, constant low concentrations result in a slow WNT upregulation, and therefore the signal trajectory stays in a pluripotency or ExE-promoting region for too long and does not efficiently promote mesoderm differentiation (Figures 7C and S12A–S12C). Taken together, the model unveils a strategy for efficiently inducing mesoderm with BMP: induction with a high BMP dose that rapidly increases endogenous WNT signaling, after which BMP must be withdrawn for cells to become mesoderm over ExE.

As we mentioned above, a recent approach based on the Waddington landscape metaphor has been shown to be a powerful yet simple way to study cell fate transitions in different contexts.[49–56] In these high-level, low-dimensional models, the differentiation of a cell is depicted as a trajectory on a landscape. The basins or attractors of the landscape represent the different cell types the cell can differentiate into. In particular, we and others have shown that using dynamical systems theory, one can enumerate the possible bifurcations and link the parameters of these bifurcations to the levels of signals to build the landscape model, which then can be quantitatively fitted to the data.[49,55] However, no studies have yet linked the modeled dynamics of a cell moving on the landscape with measured signaling or gene expression dynamics of the type we have measured here, and the CFN model proposed incorporates this data in a straightforward way. Although there is still no analytical method to compare low-dimensional landscape models and higher-dimensional, more mechanistic models such as that proposed here, we wondered whether we could leverage our results to understand which landscape geometries are compatible with our proposed CFN model that, although phenomenological, is built on mechanistic knowledge of signaling interactions.

We investigated how the data constrained the geometry of the fate map or underlying low-dimensional landscape. For this purpose, we generated fate maps for different parameters accepted in the Monte Carlo optimization algorithm. We observed three main classes of fate map configurations (see appendix in supplemental information for more details). In the starting configuration, the attractor corresponding to the ExE fate is always present for all signaling regimes, and the values of the signals control the presence of the pluripotent and/or mesoderm attractor. In particular, under low BMP levels, WNT controls a bistable switch between the pluripotent and mesoderm attractors, and as BMP increases, both the pluripotent and mesoderm attractors bifurcate away. As the fitting improved, this configuration evolved, and the bistable switch controlling the presence of the pluripotent and mesoderm attractors disappeared, becoming a smooth transition instead. Finally, a last and best-fitting configuration involved transitions between all combinations of pairs of attractors, resembling the transitions that can be observed in the elliptic umbilic catastrophe (Figures 7 and S12D; see appendix in supplemental information). Interestingly, a connection between a three mutually repulsive state network and the elliptic umbilic catastrophe had been proposed before,[60] but, to our knowledge, this is the first experimental system that confirms this idea.

Here, we have shown that by pulsing BMP signaling, we can obtain a relatively high population of cells that exclusively expresses the mesoderm marker BRA after 2 days. However, this population is heterogeneous, and we speculated that this was due to the limitations of the dynamics of endogenous WNT in response to BMP. Inducing hPSCs by CHIR results in a strong, rapid, and sustained WNT response[40] and yields a very high fraction of mesoderm cells (Figure S12E). However, this induction is slow, and most of the cells still express SOX2 after 2 days of induction (Figures 7E and S11), and a homogeneous mesodermal population only emerges after 3 days (Figure S12E). Modeling CHIR through β-catenin activation (Figure 4), we could reproduce this effect (Figures 7D and 7E, yellow condition). We wondered whether we could take advantage of the insights above to speed up mesoderm induction by CHIR. Our goal was to find a 2-day protocol that yielded the highest BRA expression by varying a sequence of inductions with BMP and CHIR. Our model suggested that the induction of mesoderm by CHIR was slow because of a strong SOX2 inhibition of the mesoderm state. We reasoned that a pulse of BMP4 signal could be used to destabilize the pluripotency state, which, if then followed by CHIR induction, could yield higher mesoderm expression by 48 h. Our model predicted that a 4 h pulse of BMP was sufficient for this purpose and, if followed by 44 h of CHIR treatment, would result in a very high BRA expression by day 2 (Figures 7D and 7E, red condition). Indeed, experimentally, by day 2, we obtained higher BRA expression and much more complete SOX2 downregulation than with CHIR alone (Figure 7E, yellow condition). Differences in variances between experimental and simulated distributions were expected due to convergence to attractors in the simulations. Despite this, the trends in the simulations and the data are similar. Therefore, the model explains the combinatorial effect between BMP and Wnt signals in mediating decisions between the pluripotent, mesoderm, and ExE fates and offers a platform to rationally design more optimal protocols. Taken together, our study highlights how understanding signaling dynamics can be exploited for developing efficient differentiation protocols.

DISCUSSION

In this study, we have unveiled a combinatorial mechanism by which BMP and downstream endogenous WNT signaling combinatorially control the cell state transitions observed in mammalian gastrulation and previous *in vitro* studies. We showed that the logic of this BMP-WNT circuit causes the decision between mesoderm and extraembryonic to depend primarily on the duration of signaling. In particular, a specific pulse of high concentration of BMP4 signal is much more efficient at inducing a mesoderm-like state than any constant concentration. Taking advantage of signaling and fate reporter cell lines, we showed that these results depend on an endogenous BMP-induced WNT bistability. A simple minimal CFN model explains how the observed cell state transitions are regulated by combinatorial interpretation of these two signals. Induction with a short BMP pulse is insufficient to induce endogenous WNT signaling, resulting in hPSCs remaining in the initial pluripotent state. On the contrary, long pulses of high BMP4 concentration induce endogenous WNT signals, but a high BMP signal overrides the endogenous WNT, resulting in extraembryonic differentiation. A pulse of BMP4 of intermediate length that activates WNT autoregulation results in efficient mesoderm differentiation. At lower constant concentrations, WNT activation is slow, and cells are therefore pushed toward an ExE fate before experiencing this signal, explaining why low doses of BMP are not interchangeable with a pulse of a high BMP dose. Taken together, our study reveals an underlying logic where, to induce efficient mesodermal induction, BMP signaling needs to be sufficiently strong to rapidly induce endogenous WNT signaling upregulation but sufficiently short for cells to differentiate in a low BMP, high WNT environment.

Our work adds to the growing body of knowledge on how the dynamics of signals are interpreted by downstream regulatory networks. Broadly, these interpretations can be categorized into two distinct types, depending on whether duration and concentration are interchangeable (i.e., cells primarily interpret the integral of the signal over time) or whether additional information to the integral of the input signal is decoded by the downstream gene regulatory network. Several examples have been shown of the first case, such as glucose sensing in plants[61] or the interpretation of Shh signaling in the murine neural tube,[23] where there is an effective trade-off between duration and concentration, so that shorter durations at higher concentration are sufficient to induce the same fates as longer exposure to lower concentrations. It is of particular interest to investigate the mechanisms by which cells interpret additional information in the dynamics of the inductive signal beyond the integral, and several instances of this case have been shown in different contexts. For example, in the case of NF-κB, it was shown that, while the integral of the signal controls the activation of a downstream regulatory program in a switch-like fashion, it is the strength of the pulse that controls the percentage of cells that are activated.[32] NF-κB signaling also activates different classes of genes depending on the duration of signaling with some genes responding immediately while another class requires sustained activation.[31] Interestingly, in that case, the early responding genes require only a very transient initial pulse to achieve nearly a full response, while sustained signaling is required to activate a set of late targets. By contrast, in the case studied here, the direct result of activation, including expression of genes such as GATA3 and extraembryonic differentiation, required sustained activation, while secondary outputs, such as mesoderm differentiation, require a transient pulse of the signal. This demonstrates that downstream regulatory logic can implement diverse relationships between signaling dynamics and phenotypic outputs.

The three-way decision between pluripotent, primitive streak mesoderm, and extraembryonic amnion is more complex than integral regulation or that studied in the context of NF-κB. It relies on the interplay between BMP and Wnt signaling and cannot be predicted by a parameter of any one of these pathways. Interestingly, we observed that the initial decrease in SOX2 correlated very well with the cumulative integral of BMP signaling as measured by SMAD4 across several different time courses of applied BMP signal (Figure S10E). This suggests that in our system, while the initial dissolution of the pluripotent state by BMP signaling may indeed by controlled by the integral of signaling, the decision between different potential fates relies on the interpretation of multiple pathways. Indeed, when Wnt signaling is inhibited so that cells can only switch from the pluripotent to the extraembryonic fate, the fraction of cells adopting this fate is well predicted by the integral of the BMP signal.[38]

It is also important to note that measuring the intensity of signaling with a reporter is essential, as the external concentration does not translate directly into signaling activity. In the case of BMP signaling, the activation of the SMAD proteins is switch-like and regulated over a narrow range of concentrations, so it is difficult to regulate the effective activity simply by changing the concentration of ligand in the media.[39] Further, the loss of the BMP from the media over time causes more prolonged signaling at higher doses,[39] making it difficult to decouple duration from concentration. Together, these features mean that even though the dissolution of pluripotency is responsive to the integral of signaling, in practice, the duration of the signal is more easily controlled and is more likely to be the determining factor *in vivo*.

It has recently been proposed that BMP4 differentiation rapidly becomes irreversible due to positive feedback through GATA3.[62] In that study, a 1 h pulse of BMP4 was sufficient to induce irreversible differentiation in hPSC colonies, which is in clear contradiction with our results (Figures 1, 2, S1, and S2). Irreversible differentiation following short exposure to BMP is contradictory to several studies from our lab and others[14,15,22,63] that showed that BMP signaling is rapidly downregulated by small molecule or extracellular protein inhibitors and that pulses of longer than 10 or 24 h are needed to induce differentiation in both in micropatterned colonies and regular culture, respectively. Apparently irreversible differentiation is likely due to incomplete removal of the BMP in the media (Figures S2C and S2D). Indeed, we found using a live-cell reporter for BMP signaling that signaling activity remained substantially above baseline when media containing high doses of BMP was replaced by media alone; however, treatment with Noggin quickly abrogated this continued signaling. Further experiments with washing confirmed that BMP ligands cannot be removed from the media by washing alone (see Figures S2C and S2D).

Our results showed that, under BMP induction of hPSCs, there is a relatively narrow window of durations of BMP exposure that is able to specify mesoderm, and this was related to the dynamics of the induced endogenous WNT signaling. This highlights the need to consider dynamics when developing *in vitro* differentiation protocols. In particular, our study focused on the duration of a single pulse of BMP, but more complex time courses of BMP stimulation are possible, and it would be interesting to determine the optimal time courses for achieving different fates. *In vivo*, although the same cascade of signals controls gastrulation in other mammals, the developmental time scales vary widely. It is unclear how the window of BMP duration needed might be matched to the developmental time scale. Interestingly, recent studies have uncovered cell movement as a mechanism that controls the temporal exposure to morphogens.[64] Further work could elucidate whether the differences might be due to differential protein stability and cell cycle duration, as has been recently proposed in other contexts.[65,66]

We show that there is a form of memory in the WNT signaling so that transient exposure to BMP can be sufficient to induce WNT in a sustained fashion. This is reminiscent of the interplay between WNT and NODAL signaling in which cells remember prior exposure to WNT, which alters their subsequent response to NODAL.[67,68] The mechanisms are different as, in the case described here, BMP leads to ongoing WNT signaling, likely through sustained expression of WNT ligands, while WNT affects the interpretation of NODAL by inducing EOMES without a subsequent requirement for the continuation of WNT activity.

Much work has been done to decipher the dynamics of signals that control the patterning of micropatterned hPSC colonies treated with BMP4.[14,15,17,39] These studies have unveiled that, initially, there is a homogeneous response to BMP4 across the whole colony, which is restricted to the edge via receptor localization and accumulation of Noggin at the colony center between 10 and 20 h after treatment.[15,39] Subsequently, around 30 h, waves of WNT and Nodal signaling start near the edge of the colony and move inward, spatially correlating with a ring of BRA-positive mesodermal cells.[14,39] Although our results have been obtained in a culture with lower cell density where self-organized patterning does not occur, they are consistent with the observations of a pulse of BMP throughout the colony, which induces endogenous WNT signal. The cells that adopt a mesodermal fate are those that are displaced from the edge and, therefore, only experience transient BMP signaling followed by upregulation of Wnt signaling to high levels. Thus, the model developed here could be a good starting point for building a spatial model to understand how patterns arise from the interplay of dynamic signaling and combinatorial interpretation.

STAR★METHODS

Detailed methods are provided in the online version of this paper and include the following:

- KEY RESOURCES TABLE
- RESOURCE AVAILABILITY
  - Lead contact
  - Materials availability
  - Data and code availability
- EXPERIMENTAL MODEL AND STUDY PARTICIPANT DETAILS
  - Cell lines
- METHOD DETAILS
  - Cell culture, treatments, and differentiation
  - Plasmids and generation of SOX2-mCitrine-labeled hPSC cell line
  - Immunofluorescence antibody staining
  - RNA sequencing
  - Image acquisition
- QUANTIFICATION AND STATISTICAL ANALYSIS
  - RNA sequencing quantification
  - Image analysis
  - Cell fate classification
  - Mathematical models

SUPPLEMENTAL INFORMATION

Supplemental information can be found online at https://doi.org/10.1016/j.cels.2024.04.001.

ACKNOWLEDGMENTS

We thank Idse Heemskerk, Seth Teague, Francisco-Jesús Castro-Jiménez, Nathan Lord, Luciano Marcon, and Eric Siggia for helpful discussions on the project. We thank the Brivanlou lab for sharing the plasmids used to create the SOX2::mCitrine cell line, Sapna Chhabra for performing the experiment in Figure S8C and for helpful feedback on the project, Joseph Massey for sharing helpful pieces of code for analyzing live-cell imaging data, Lizhong Liu for technical assistance when creating the SOX2::mCitrine, and all the members of the Warmflash lab for helpful feedback. This work was supported by grants to M.A.O.-S. from CONACYT (Consejo Nacional de Ciencia y Tecnología. México) and to A.W. from the National Science Foundation (MCB-1553228 and MCB-2135296), the Simons Foundation (511079), and NIGMS (R35GM149328).

AUTHOR CONTRIBUTIONS

E.C.-A.: conceptualization, methodology, investigation, validation, software, formal analysis, data curation, visualization, supervision, writing – original draft, and writing – review & editing. S.T.Y.: investigation and validation. M.A.O.-S. (micropatterning experiment): investigation, software, formal analysis, data curation, visualization, and writing – review & editing. S.D. (RNA sequencing experiment): investigation, software, and writing – review & editing. M.C.G.: investigation. A.W.: conceptualization, methodology, supervision, funding acquisition, project administration, writing – original draft, and writing – review & editing.

DECLARATION OF INTERESTS

A.W. is a cofounder of and holds equity in Simbryo Technologies. The work presented here is not related to the interests of this commercial entity.

Received: March 2, 2023
Revised: October 10, 2023
Accepted: April 10, 2024
Published: April 30, 2024

REFERENCES

1. Arnold, S.J., and Robertson, E.J. (2009). Making a commitment: cell lineage allocation and axis patterning in the early mouse embryo. Nat. Rev. Mol. Cell Biol. *10*, 91–103. https://doi.org/10.1038/nrm2618.
2. Bardot, E.S., and Hadjantonakis, A.K. (2020). Mouse gastrulation: coordination of tissue patterning, specification and diversification of cell fate. Mech. Dev. *163*, 103617. https://doi.org/10.1016/j.mod.2020.103617.
3. Ben-Haim, N., Lu, C., Guzman-Ayala, M., Pescatore, L., Mesnard, D., Bischofberger, M., Naef, F., Robertson, E.J., and Constam, D.B. (2006). The nodal precursor acting via activin receptors induces mesoderm by maintaining a source of its convertases and BMP4. Dev. Cell *11*, 313–323. https://doi.org/10.1016/j.devcel.2006.07.005.
4. Brennan, J., Lu, C.C., Norris, D.P., Rodriguez, T.A., Beddington, R.S.P., and Robertson, E.J. (2001). Nodal signalling in the epiblast patterns the early mouse embryo. Nature *411*, 965–969. https://doi.org/10.1038/35082103.
5. Tortelote, G.G., Hernández-Hernández, J.M., Quaresma, A.J.C., Nickerson, J.A., Imbalzano, A.N., and Rivera-Pérez, J.A. (2013). Wnt3 function in the epiblast is required for the maintenance but not the initiation of gastrulation in mice. Dev. Biol. *374*, 164–173. https://doi.org/10.1016/j.ydbio.2012.10.013.
6. Conlon, F.L., Lyons, K.M., Takaesu, N., Barth, K.S., Kispert, A., Herrmann, B., and Robertson, E.J. (1994). A primary requirement for nodal in the

formation and maintenance of the primitive streak in the mouse. Development *120*, 1919–1928. https://doi.org/10.1242/dev.120.7.1919.

7. Liu, P., Wakamiya, M., Shea, M.J., Albrecht, U., Behringer, R.R., and Bradley, A. (1999). Requirement for Wnt3 in vertebrate axis formation. Nat. Genet. *22*, 361–365. https://doi.org/10.1038/11932.
8. Winnier, G., Blessing, M., Labosky, P.A., and Hogan, B.L. (1995). Bone morphogenetic protein-4 is required for mesoderm formation and patterning in the mouse. Genes Dev. *9*, 2105–2116. https://doi.org/10.1101/gad.9.17.2105.
9. Camacho-Aguilar, E., and Warmflash, A. (2020). Insights into mammalian morphogen dynamics from embryonic stem cell systems. Curr. Top. Dev. Biol. *137*, 279–305. https://doi.org/10.1016/bs.ctdb.2019.11.010.
10. Fu, J., Warmflash, A., and Lutolf, M.P. (2021). Stem-cell-based embryo models for fundamental research and translation. Nat. Mater. *20*, 132–144. https://doi.org/10.1038/s41563-020-00829-9.
11. Heemskerk, I. (2020). Full of potential: Pluripotent stem cells for the systems biology of embryonic patterning. Dev. Biol. *460*, 86–98. https://doi.org/10.1016/j.ydbio.2019.05.004.
12. Shahbazi, M.N., Siggia, E.D., and Zernicka-Goetz, M. (2019). Self-organization of stem cells into embryos: A window on early mammalian development. Science *364*, 948–951. https://doi.org/10.1126/science.aax0164.
13. Chhabra, S., and Warmflash, A. (2021). BMP-treated human embryonic stem cells transcriptionally resemble amnion cells in the monkey embryo. Biol. Open *10*, bio058617. https://doi.org/10.1242/bio.058617.
14. Chhabra, S., Liu, L., Goh, R., Kong, X., and Warmflash, A. (2019). Dissecting the dynamics of signaling events in the BMP, WNT, and NODAL cascade during self-organized fate patterning in human gastruloids. PLoS Biol. *17*, e3000498. https://doi.org/10.1371/journal.pbio.3000498.
15. Etoc, F., Metzger, J., Ruzo, A., Kirst, C., Yoney, A., Ozair, M.Z., Brivanlou, A.H., and Siggia, E.D. (2016). A Balance between Secreted Inhibitors and Edge Sensing Controls Gastruloid Self-Organization. Dev. Cell *39*, 302–315. https://doi.org/10.1016/J.DEVCEL.2016.09.016.
16. Minn, K.T., Fu, Y.C., He, S., Dietmann, S., George, S.C., Anastasio, M.A., Morris, S.A., and Solnica-Krezel, L. (2020). High-resolution transcriptional and morphogenetic profiling of cells from micropatterned human ESC gastruloid cultures. eLife *9*, e59445. https://doi.org/10.7554/eLife.59445.
17. Warmflash, A., Sorre, B., Etoc, F., Siggia, E.D., and Brivanlou, A.H. (2014). A method to recapitulate early embryonic spatial patterning in human embryonic stem cells. Nat. Methods *11*, 847–854. https://doi.org/10.1038/nmeth.3016.
18. Shao, Y., Taniguchi, K., Gurdziel, K., Townshend, R.F., Xue, X., Yong, K.M.A., Sang, J., Spence, J.R., Gumucio, D.L., and Fu, J. (2017). Self-organized amniogenesis by human pluripotent stem cells in a biomimetic implantation-like niche. Nat. Mater. *16*, 419–425. https://doi.org/10.1038/nmat4829.
19. Shao, Y., Taniguchi, K., Townshend, R.F., Miki, T., Gumucio, D.L., and Fu, J. (2017). A pluripotent stem cell-based model for post-implantation human amniotic sac development. Nat. Commun. *8*, 208. https://doi.org/10.1038/s41467-017-00236-w.
20. Guo, G., Stirparo, G.G., Strawbridge, S.E., Spindlow, D., Yang, J., Clarke, J., Dattani, A., Yanagida, A., Li, M.A., Myers, S., et al. (2021). Human naive epiblast cells possess unrestricted lineage potential. Cell Stem Cell *28*, 1040–1056.e6. https://doi.org/10.1016/j.stem.2021.02.025.
21. Wolpert, L. (1969). Positional information and the spatial pattern of cellular differentiation. J. Theor. Biol. *25*, 1–47. https://doi.org/10.1016/S0022-5193(69)80016-0.
22. Nemashkalo, A., Ruzo, A., Heemskerk, I., and Warmflash, A. (2017). Morphogen and community effects determine cell fates in response to BMP4 signaling in human embryonic stem cells. Development *144*, 3042–3053. https://doi.org/10.1242/dev.153239.
23. Dessaud, E., Yang, L.L., Hill, K., Cox, B., Ulloa, F., Ribeiro, A., Mynett, A., Novitch, B.G., and Briscoe, J. (2007). Interpretation of the sonic hedgehog morphogen gradient by a temporal adaptation mechanism. Nature *450*, 717–720. https://doi.org/10.1038/nature06347.
24. Economou, A.D., and Hill, C.S. (2020). Temporal dynamics in the formation and interpretation of Nodal and BMP morphogen gradients. Curr. Top. Dev. Biol. *137*, 363–389. https://doi.org/10.1016/bs.ctdb.2019.10.012.
25. Economou, A.D., Guglielmi, L., East, P., and Hill, C.S. (2022). Nodal signaling establishes a competency window for stochastic cell fate switching. Dev. Cell *57*, 2604–2622.e5. https://doi.org/10.1016/j.devcel.2022.11.008.
26. Green, J.B.A., Howes, G., Symes, K., Cooke, J., and Smith, J.C. (1990). The biological effects of XTC-MIF: quantitative comparison with Xenopus bFGF. Development *108*, 173–183. https://doi.org/10.1242/dev.108.1.173.
27. Huang, A., and Saunders, T.E. (2020). A matter of time: Formation and interpretation of the Bicoid morphogen gradient. Curr. Top. Dev. Biol. *137*, 79–117. https://doi.org/10.1016/bs.ctdb.2019.11.016.
28. Pagès, F., and Kerridge, S. (2000). Morphogen gradients: a question of time or concentration? Trends Genet. *16*, 40–44. https://doi.org/10.1016/S0168-9525(99)01880-6.
29. Sagner, A., and Briscoe, J. (2017). Morphogen interpretation: concentration, time, competence, and signaling dynamics. Wiley Interdiscip. Rev. Dev. Biol. *6*, e271. https://doi.org/10.1002/wdev.271.
30. Sako, K., Pradhan, S.J., Barone, V., Inglés-Prieto, Á., Müller, P., Ruprecht, V., Čapek, D., Galande, S., Janovjak, H., and Heisenberg, C.P. (2016). Optogenetic Control of Nodal Signaling Reveals a Temporal Pattern of Nodal Signaling Regulating Cell Fate Specification during Gastrulation. Cell Rep. *16*, 866–877. https://doi.org/10.1016/j.celrep.2016.06.036.
31. Hoffmann, A., Levchenko, A., Scott, M.L., and Baltimore, D. (2002). The IkappaB-NF-kappaB signaling module: temporal control and selective gene activation. Science *298*, 1241–1245. https://doi.org/10.1126/science.1071914.
32. Kellogg, R.A., Tian, C., Lipniacki, T., Quake, S.R., and Tay, S. (2015). Digital signaling decouples activation probability and population heterogeneity. eLife *4*, e08931. https://doi.org/10.7554/eLife.08931.
33. Lee, R.E.C., Qasaimeh, M.A., Xia, X., Juncker, D., and Gaudet, S. (2016). NF-κB signalling and cell fate decisions in response to a short pulse of tumour necrosis factor. Sci. Rep. *6*, 39519. https://doi.org/10.1038/srep39519.
34. Tay, S., Hughey, J.J., Lee, T.K., Lipniacki, T., Quake, S.R., and Covert, M.W. (2010). Single-cell NF-κB dynamics reveal digital activation and analogue information processing. Nature *466*, 267–271. https://doi.org/10.1038/nature09145.
35. Lahav, G., Rosenfeld, N., Sigal, A., Geva-Zatorsky, N., Levine, A.J., Elowitz, M.B., and Alon, U. (2004). Dynamics of the p53-Mdm2 feedback loop in individual cells. Nat. Genet. *36*, 147–150. https://doi.org/10.1038/ng1293.
36. Martyn, I., Kanno, T.Y., Ruzo, A., Siggia, E.D., and Brivanlou, A.H. (2018). Self-organization of a human organizer by combined Wnt and Nodal signalling. Nature *558*, 132–135. https://doi.org/10.1038/s41586-018-0150-y.
37. Zhang, P., Li, J., Tan, Z., Wang, C., Liu, T., Chen, L., Yong, J., Jiang, W., Sun, X., Du, L., et al. (2008). Short-term BMP-4 treatment initiates mesoderm induction in human embryonic stem cells. Blood *111*, 1933–1941. https://doi.org/10.1182/blood-2007-02-074120.
38. Teague, S., Primavera, G., Chen, B., Liu, Z.Y., Yao, L., Freeburne, E., Khan, H., Jo, K., Johnson, C., and Heemskerk, I. (2024). Time-integrated BMP signaling determines fate in a stem cell model for early human development. Nat. Commun. *15*, 1471. https://doi.org/10.1038/s41467-024-45719-9.
39. Heemskerk, I., Burt, K., Miller, M., Chhabra, S., Guerra, M.C., Liu, L., and Warmflash, A. (2019). Rapid changes in morphogen concentration control self-organized patterning in human embryonic stem cells. eLife *8*, e40526. https://doi.org/10.7554/eLife.40526.

40. Massey, J., Liu, Y., Alvarenga, O., Saez, T., Schmerer, M., and Warmflash, A. (2019). Synergy with TGFβ ligands switches WNT pathway dynamics from transient to sustained during human pluripotent cell differentiation. Proc. Natl. Acad. Sci. USA *116*, 4989–4998. https://doi.org/10.1073/pnas.1815363116.

41. Wang, J., Sinha, T., and Wynshaw-Boris, A. (2012). Wnt Signaling in Mammalian Development: Lessons from Mouse Genetics. Cold Spring Harb. Perspect. Biol. *4*, a007963. https://doi.org/10.1101/cshperspect.a007963.

42. Kurek, D., Neagu, A., Tastemel, M., Tüysüz, N., Lehmann, J., van de Werken, H.J.G., Philipsen, S., van der Linden, R., van Maas, A., van IJcken, W.F.J., et al. (2015). Endogenous WNT Signals Mediate BMP-Induced and Spontaneous Differentiation of Epiblast Stem Cells and Human Embryonic Stem Cells. Stem Cell Rep. *4*, 114–128. https://doi.org/10.1016/j.stemcr.2014.11.007.

43. Blassberg, R., Patel, H., Watson, T., Gouti, M., Metzis, V., Delás, M.J., and Briscoe, J. (2022). Sox2 levels regulate the chromatin occupancy of WNT mediators in epiblast progenitors responsible for vertebrate body formation. Nat. Cell Biol. *24*, 633–644. https://doi.org/10.1038/s41556-022-00910-2.

44. Lacoste, A., Berenshteyn, F., and Brivanlou, A.H. (2009). An Efficient and Reversible Transposable System for Gene Delivery and Lineage-Specific Differentiation in Human Embryonic Stem Cells. Cell Stem Cell *5*, 332–342. https://doi.org/10.1016/j.stem.2009.07.011.

45. Chickarmane, V., Olariu, V., and Peterson, C. (2012). Probing the role of stochasticity in a model of the embryonic stem cell – heterogeneous gene expression and reprogramming efficiency. BMC Syst. Biol. *6*, 98. https://doi.org/10.1186/1752-0509-6-98.

46. Gouti, M., Delile, J., Stamataki, D., Wymeersch, F.J., Huang, Y., Kleinjung, J., Wilson, V., and Briscoe, J. (2017). A Gene Regulatory Network Balances Neural and Mesoderm Specification during Vertebrate Trunk Development. Dev. Cell *41*, 243–261.e7. https://doi.org/10.1016/j.devcel.2017.04.002.

47. Karlebach, G., and Shamir, R. (2008). Modelling and analysis of gene regulatory networks. Nat. Rev. Mol. Cell Biol. *9*, 770–780. https://doi.org/10.1038/nrm2503.

48. Verd, B., Crombach, A., and Jaeger, J. (2017). Dynamic Maternal Gradients Control Timing and Shift-Rates for Drosophila Gap Gene Expression. PLoS Comput. Biol. *13*, e1005285. https://doi.org/10.1371/journal.pcbi.1005285.

49. Camacho-Aguilar, E., Warmflash, A., and Rand, D.A. (2021). Quantifying cell transitions in C. elegans with data-fitted landscape models. PLoS Comput. Biol. *17*, e1009034. https://doi.org/10.1371/journal.pcbi.1009034.

50. Coomer, M.A., Ham, L., and Stumpf, M.P.H. (2022). Noise distorts the epigenetic landscape and shapes cell-fate decisions. Cell Syst. *13*, 83–102.e6. https://doi.org/10.1016/j.cels.2021.09.002.

51. Corson, F., and Siggia, E.D. (2012). Geometry, epistasis, and developmental patterning. Proc. Natl. Acad. Sci. USA *109*, 5568–5575. https://doi.org/10.1073/pnas.1201505109.

52. Corson, F., and Siggia, E.D. (2017). Gene-free methodology for cell fate dynamics during development. eLife *6*, e30743. https://doi.org/10.7554/eLife.30743.

53. Huang, S. (2012). The molecular and mathematical basis of Waddington's epigenetic landscape: A framework for post-Darwinian biology? BioEssays *34*, 149–157. https://doi.org/10.1002/bies.201100031.

54. Mojtahedi, M., Skupin, A., Zhou, J., Castaño, I.G., Leong-Quong, R.Y.Y., Chang, H., Trachana, K., Giuliani, A., and Huang, S. (2016). Cell Fate Decision as High-Dimensional Critical State Transition. PLoS Biol. *14*, e2000640. https://doi.org/10.1371/journal.pbio.2000640.

55. Sáez, M., Blassberg, R., Camacho-Aguilar, E., Siggia, E.D., Rand, D.A., and Briscoe, J. (2022). Statistically derived geometrical landscapes capture principles of decision-making dynamics during cell fate transitions. Cell Syst. *13*, 12–28.e3. https://doi.org/10.1016/j.cels.2021.08.013.

56. Valcourt, J.R., Huang, R.E., Kundu, S., Venkatasubramanian, D., Kingston, R.E., and Ramanathan, S. (2021). Modulating mesendoderm competence during human germ layer differentiation. Cell Rep. *37*, 109990. https://doi.org/10.1016/j.celrep.2021.109990.

57. Li, Y., Moretto-Zita, M., Soncin, F., Wakeland, A., Wolfe, L., Leon-Garcia, S., Pandian, R., Pizzo, D., Cui, L., Nazor, K., et al. (2013). BMP4-directed trophoblast differentiation of human embryonic stem cells is mediated through a ΔNp63+ cytotrophoblast stem cell state. Development *140*, 3965–3976. https://doi.org/10.1242/dev.092155.

58. Xu, R.H., Chen, X., Li, D.S., Li, R., Addicks, G.C., Glennon, C., Zwaka, T.P., and Thomson, J.A. (2002). BMP4 initiates human embryonic stem cell differentiation to trophoblast. Nat. Biotechnol. *20*, 1261–1264. https://doi.org/10.1038/nbt761.

59. Yang, R., Goedel, A., Kang, Y., Si, C., Chu, C., Zheng, Y., Chen, Z., Gruber, P.J., Xiao, Y., Zhou, C., et al. (2021). Amnion signals are essential for mesoderm formation in primates. Nat. Commun. *12*, 5126. https://doi.org/10.1038/s41467-021-25186-2.

60. Rand, D.A., Raju, A., Sáez, M., Corson, F., and Siggia, E.D. (2021). Geometry of gene regulatory dynamics. Proc. Natl. Acad. Sci. USA *118*, e2109729118. https://doi.org/10.1073/pnas.2109729118.

61. Fu, Y., Lim, S., Urano, D., Tunc-Ozdemir, M., Phan, N.G., Elston, T.C., and Jones, A.M. (2014). Reciprocal Encoding of Signal Intensity and Duration in a Glucose-Sensing Circuit. Cell *156*, 1084–1095. https://doi.org/10.1016/j.cell.2014.01.013.

62. Gunne-Braden, A., Sullivan, A., Gharibi, B., Sheriff, R.S.M., Maity, A., Wang, Y.F., Edwards, A., Jiang, M., Howell, M., Goldstone, R., et al. (2020). GATA3 Mediates a Fast, Irreversible Commitment to BMP4-Driven Differentiation in Human Embryonic Stem Cells. Cell Stem Cell *26*, 693–706.e9. https://doi.org/10.1016/j.stem.2020.03.005.

63. Jo, K., Teague, S., Chen, B., Khan, H.A., Freeburne, E., Li, H., Li, B., Ran, R., Spence, J.R., and Heemskerk, I. (2022). Efficient differentiation of human primordial germ cells through geometric control reveals a key role for Nodal signaling. eLife *11*, e72811. https://doi.org/10.7554/eLife.72811.

64. Fulton, T., Spiess, K., Thomson, L., Wang, Y., Clark, B., Hwang, S., Paige, B., Verd, B., and Steventon, B. (2022). Cell Rearrangement Generates Pattern Emergence as a Function of Temporal Morphogen Exposure. Preprint at bioRxiv. https://doi.org/10.1101/2021.02.05.429898.

65. Matsuda, M., Hayashi, H., Garcia-Ojalvo, J., Yoshioka-Kobayashi, K., Kageyama, R., Yamanaka, Y., Ikeya, M., Toguchida, J., Alev, C., and Ebisuya, M. (2020). Species-specific segmentation clock periods are due to differential biochemical reaction speeds. Science *369*, 1450–1455. https://doi.org/10.1126/science.aba7668.

66. Rayon, T., Stamataki, D., Perez-Carrasco, R., Garcia-Perez, L., Barrington, C., Melchionda, M., Exelby, K., Lazaro, J., Tybulewicz, V.L.J., Fisher, E.M.C., et al. (2020). Species-specific pace of development is associated with differences in protein stability. Science *369*, eaba7667. https://doi.org/10.1126/science.aba7667.

67. Yoney, A., Etoc, F., Ruzo, A., Carroll, T., Metzger, J.J., Martyn, I., Li, S., Kirst, C., Siggia, E.D., and Brivanlou, A.H. (2018). WNT signaling memory is required for ACTIVIN to function as a morphogen in human gastruloids. eLife *7*, 1–28. https://doi.org/10.7554/eLife.38279.

68. Yoney, A., Bai, L., Brivanlou, A.H., and Siggia, E.D. (2022). Mechanisms underlying WNT-mediated priming of human embryonic stem cells. Development *149*, dev200335. https://doi.org/10.1242/dev.200335.

69. Deglincerti, A., Etoc, F., Guerra, M.C., Martyn, I., Metzger, J., Ruzo, A., Simunovic, M., Yoney, A., Brivanlou, A.H., Siggia, E., and Warmflash, A. (2016). Self-organization of human embryonic stem cells on micropatterns. Nat. Protoc. *11*, 2223–2232. https://doi.org/10.1038/nprot.2016.131.

70. Patro, R., Duggal, G., Love, M.I., Irizarry, R.A., and Kingsford, C. (2017). Salmon provides fast and bias-aware quantification of transcript expression. Nat. Methods *14*, 417–419. https://doi.org/10.1038/nmeth.4197.

71. Love, M.I., Soneson, C., Hickey, P.F., Johnson, L.K., Pierce, N.T., Shepherd, L., Morgan, M., and Patro, R. (2020). Tximeta: Reference

sequence checksums for provenance identification in RNA-seq. PLoS Comput. Biol. *16*, e1007664. https://doi.org/10.1371/journal.pcbi.1007664.

72. Berg, S., Kutra, D., Kroeger, T., Straehle, C.N., Kausler, B.X., Haubold, C., Schiegg, M., Ales, J., Beier, T., Rudy, M., et al. (2019). ilastik: interactive machine learning for (bio)image analysis. Nat. Methods *16*, 1226–1232. https://doi.org/10.1038/s41592-019-0582-9.

73. Sommer, C., Straehle, C., Köthe, U., and Hamprecht, F.A. (2011). Ilastik: Interactive learning and segmentation toolkit. In IEEE International Symposium on Biomedical Imaging: From Nano to Macro, pp. 230–233. https://doi.org/10.1109/ISBI.2011.5872394.

74. Preibisch, S., Saalfeld, S., and Tomancak, P. (2009). Globally optimal stitching of tiled 3D microscopic image acquisitions. Bioinformatics *25*, 1463–1465. https://doi.org/10.1093/bioinformatics/btp184.

STAR★METHODS

KEY RESOURCES TABLE

REAGENT or RESOURCE	SOURCE	IDENTIFIER
Antibodies		
Rabbit monoclonal Anti-SOX2	Cell Signaling Technology	Cat# 23064s, RRID: AB_2714146
Goat polyclonal Anti-Brachyury	R&D Systems	Cat# AF2085, RRID: AB_2200235
Rabbit monoclonal Anti-Brachyury	R&D Systems	Cat# MAB20851
Mouse monoclonal Anti-CDX2	Biogenex	Cat# MU392A, RRID: AB_2923402
Mouse monoclonal Anti-ISL1	DSHB	Cat# 39.4D5, RRID: AB_2314683
Mouse monoclonal Anti-OCT3/4	BD Biosciences	Cat# 611203, RRID: AB_398737
Mouse monoclonal Anti-NANOG	BD Biosciences	Cat# 560482, RRID: AB_1645598
Goat polyclonal Anti-NANOG	R&D Systems	Cat# AF1997, RRID: AB_355097
Goat polyclonal Anti-HAND1	R&D Systems	Cat# AF3168, RRID: AB_2115853
Rabbit polyclonal Anti-GATA3	Thermo Fisher Scientific	Cat# PA1-101, RRID: AB_2539874
Rabbit monoclonal Anti-LEF1	Cell Signaling Technology	Cat# 2230, RRID: AB_823558
Mouse monoclonal Anti-TFAP2A	DHSB	Cat# 3B5, RRID: AB_528084
Rabbit polyclonal Anti-EOMES	Abcam	Cat# ab23345, RRID: AB_778267
Rabbit monoclonal Anti-Phospho-Smad1/5/9	Cell Signalling Technologies	Cat# 13820, RRID: AB_2493181
Alexa Fluor 488 Donkey Anti-Goat	Thermo Fisher Scientific	Cat# A-11055, RRID: AB_2534102
Alexa Fluor 488 Donkey Anti-Mouse	Thermo Fisher Scientific	Cat# A-21202, RRID: AB_141607
Alexa Fluor 488 Donkey Anti-Rabbit	Thermo Fisher Scientific	Cat# A-21206, RRID: AB_2535792
Alexa Fluor 555 Donkey Anti-Goat	Thermo Fisher Scientific	Cat# A-21432, RRID: AB_2535853
Alexa Fluor 555 Donkey Anti-Mouse	Thermo Fisher Scientific	Cat# A-31570, RRID: AB_2536180
Alexa Fluor 555 Donkey Anti-Rabbit	Thermo Fisher Scientific	Cat# A-31572, RRID: AB_162543
Alexa Fluor 647 Donkey Anti-Goat	Thermo Fisher Scientific	Cat# A-21447, RRID: AB_2535864
Alexa Fluor 647 Donkey Anti-Mouse	Thermo Fisher Scientific	Cat# A-31571, RRID: AB_162542
Alexa Fluor 647 Donkey Anti-Rabbit	Thermo Fisher Scientific	Cat# A-31573, RRID: AB_2536183
Chemicals, peptides, and recombinant proteins		
mTeSR medium	STEMCELL Technologies	Cat# 85850
mTeSR Plus medium	STEMCELL Technologies	Cat# 100-0276
Dispase	STEMCELL Technologies	Cat# 7913
Matrigel	Corning	Cat# 354277
DMEM/F12	VWR	Cat# 45000-344
Y27672	STEMCELL Technologies	Cat# 05875
Recombinant Human Laminin 511	BioLamina	Cat# LN511-0202
Blasticidin	A.G. Scientific	Cat# B-1247-SOL
G-418	Thermo Fisher Scientific	Cat# 10131035
BMP4	R&D Systems	Cat# 314BP050
Noggin	R&D Systems	Cat# 6057-NG-100
CHIR99021	MedChem Express	Cat# HY-10182
IWP2	Stemgent	Cat# 040034
CloneR	STEMCELL Technologies	Cat# 05889
Critical commercial assays		
DNeasy Blood and Tissue Kit	Qiagen	Cat# 69504
HiSpeed Plasmid Midi Kit	Qiagen	Cat# 12643
P3 Primary Cell 4D-Nucleofector X Kit L	Lonza	Cat# V4XP-3024
Deposited data		
RNA sequencing data	Gene Expression Omnibus (GEO)	GSE245027

(*Continued on next page*)

Continued

REAGENT or RESOURCE	SOURCE	IDENTIFIER
Raw imaging data, quantifications, and code to generate figures	Figshare	Doi: https://doi.org/10.6084/m9.figshare.25145528
Experimental models: Cell lines		
ESI017	ESIBIO	RRID: CVCL_B854
RUES2 GFP::Smad4 RFP::H2B	RUES2 gifted by Ali Brivanlou (Rockefeller University)	Nemashkalo et al.[22]
ESI017 GFP::β-Catenin RFP::H2B	N/A	Massey et al.[40]
ESI017 SOX2::mCitrine CFP::H2B	N/A	This study
Oligonucleotides		
ATGGCTCTTGGCTCCATGGG	Integrated DNA Technologies	This study
TGCCGTTCTTCTGCTTGTCG	Integrated DNA Technologies	This study
AGGTGAACTTCAAGATCCGCCA	Integrated DNA Technologies	This study
TACCGGGTTTTCTCCATGCTG	Integrated DNA Technologies	This study
Recombinant DNA		
PX330-sgRNA_SOX2	Gifted by Ali Brivanlou (Rockefeller University)	AW-P45,[36]
SOX2::mCitrine::T2A::Bsd	Gifted by Ali Brivanlou (Rockefeller University)	AW-P46,[36]
ePB-Helper	Gifted by Ali Brivanlou (Rockefeller University)	AW-P27
ePB-N-Cerulean-H2B	Gifted by Ali Brivanlou (Rockefeller University)	AW-P68
Software and algorithms		
Benchling	N/A	https://benchling.com
Fiji	doi: https://doi.org/10.1038/nmeth.2019	https://fiji.sc/
Ilastik	doi:https://doi.org/10.1038/s41592-019-0582-9 and doi: https://doi.org/10.1109/ISBI.2011.5872394	https://www.ilastik.org/
Salmon	doi:https://doi.org/10.1038/nmeth.4197	Salmon v1.8.0
MATLAB	The Mathworks Inc.	https://www.mathworks.com/products/matlab.html
Image analysis code	This study	https://github.com/warmflashlab/Camacho-Aguilar2022_BMPWNT https://doi.org/10.5281/zenodo.10674656
Modelling and fitting code	This study	https://github.com/warmflashlab/Camacho-Aguilar2022_BMPWNT https://doi.org/10.5281/zenodo.10674656
RNA-sequencing analysis code	This study	https://github.com/warmflashlab/Camacho-Aguilar2022_BMPWNT https://doi.org/10.5281/zenodo.10674656

RESOURCE AVAILABILITY

Lead contact

Further information and requests for resources and reagents should be directed to and will be fulfilled by the lead contact, Aryeh Warmflash (aryeh.warmflash@rice.edu).

Materials availability

The ESI017 SOX2::mCitrine CFP::H2B cell line generated in this study is available upon request from the lead contact.

Data and code availability

- Raw and processed RNA sequencing datasets generated in this study are deposited at NCBI GEO with the following reference: GEO Submission (GSE245027). Raw and processed data, model analysis workspaces, together with the code to generate the figures in this study, are deposited at figshare (https://doi.org/10.6084/m9.figshare.25145528). Due to limitations in repository size, raw data for movies will be shared by the lead contact upon request.
- Image analysis, data analysis, and modeling code are publicly available online as of the date of publication at Github at https://github.com/warmflashlab/Camacho-Aguilar2022_BMPWNT. A permanent copy of the repository has been deposited on Zenodo (https://doi.org/10.5281/zenodo.10674656).
- Any additional information required to reanalyze the data reported in this paper is available from the lead contact upon request.

EXPERIMENTAL MODEL AND STUDY PARTICIPANT DETAILS

Cell lines

The cell lines used were ESI017 (NIHhPSC-11-0093), ESI017 GFP::β-Catenin RFP::H2B,[40] RUES2 GFP::Smad4 RFP::H2B,[22] and ESI017 SOX2::mCitrine CFP::H2B (this study). ESI017 cells were obtained directly from ESIBIO while RUES2 were a gift of Ali Brivanlou (Rockefeller University). The identity of these cells as pluripotent cells was confirmed via triple staining for pluripotency markers OCT4, SOX2, and NANOG. All cells were routinely tested for mycoplasma contamination and found negative.

METHOD DETAILS

Cell culture, treatments, and differentiation

All cell lines were maintained in pluripotency maintenance culture as described in Nemashkalo et al.[22]. ESI017 SOX2::mCitrine CFP::H2B cells were maintained in mTeSR Plus medium (STEMCELL Technologies; 100-0276) and Blasticidin (5mg/ml; A.G. Scientific; B-1247-SOL) for selection, which was removed before experiments.

Ibidi m-Slide 8 Well plates (Ibidi; 80826) were used for experiments, which were coated with Matrigel (5ml/ml; Corning; 354277) diluted in DMEM/F12 (VWR;45000-344). For all experiments, cells were seeded into mTeSR1 medium (STEMCELL Technologies; 85850) containing rock inhibitor Y27672 (10mM; STEMCELL Technologies; 05875) at a density of 4 x 10^4/cm^2 (except when noted otherwise). Treatment started 21 hours after seeding, and media was always changed every 24 hours, and when performing the indicated specific treatments.

Micropatterning experiments were performed in a 96-well plate (CYTOO) containing 700 μm circular micropatterns. Coating and seeding were done as previously described by Deglincerti et al.[69]. Briefly, wells were coated with Human Recombinant Laminin 511 (Fisher Scientific) in a 1:20 dilution in PBS with calcium and magnesium for 3 hours at 37 ºC. hESCs were then seeded as single cells and maintained in mTeSR medium. After overnight incubation, cells were treated with 50 ng/ml BMP4 (R&D systems) for 48 hours or with a 1 hour pulse of 50 ng/ml BMP4 (R&D systems), followed by incubation in mTeSR1 with or without 250 ng/ml of Noggin (Fisher Scientific).

The following recombinant proteins and small molecules were used: BMP4 (R&D Systems; 314BP050), Noggin (250ng/ml; R&D Systems; 6057-NG-100), IWP2 (3mM; Stemgent; 040034), CHIR99021 (15mM; MedChem Express; HY-10182).

Plasmids and generation of SOX2-mCitrine-labeled hPSC cell line

We used CRISPR-Cas9 technology for gene editing in the ESI017 hPSC line. We used previously published constructs to fuse mCitrine directly with SOX2 at the C-terminus of the SOX2 coding sequence.[36] The SOX2 homology donor consists of a 1-kb homology arm, an mCitrine::T2A::blasticidin cassette, and a 1-kb right homology arm. Cas9 expression plasmid, homology donor DNA (Plasmid AW-P46), and guide RNA (Plasmid AW-P45; GTGCCCGGCACGGCCATTAA) were nucleofected in hPSCs using the P3 Primary Cell 4D-Nucleofector X Kit (Lonza; V4Xp-3012), and positive transformants were selected with blasticidin (10mg/ml; A.G. Scientific; B-1247-SOL) and CloneR (STEMCELL Technologies; 05889) for two days, after which cells were passaged and single clones were handpicked and amplified. Sanger sequencing was performed to screen and confirm a successful clone (Primer sequences are listed in Table S1). After establishment, the stable line was checked for pluripotency markers, i.e. OCT4, SOX2 and NANOG expression, as well as BMP differentiation both in regular culture and micropatterning, and was found indistinguishable from WT ESI017 hPSCs.

An ePiggyBac (ePB) master vector based on the pBSSK backbone,[44] harboring transposon-specific inverted terminal repeat sequences (ITR) was modified to deliver a nuclear marker CFP::H2B (Plasmid AW-P68). ePB CFP::H2B and helper (Plasmid AW-27) were nucleofected into the established SOX2::mCitrine cell line using the P3 Primary Cell 4D-Nucleofector X Kit (Lonza; V4Xp-3012). G-418 (40ng/mL; ThermoFisher; 10131035) treatment started two days after nucleofection and lasted for at least 7 days.

Immunofluorescence antibody staining

Cells were fixed with 4% PFA and stained as described in Nemashkalo et al.[22]. Antibodies and dilutions used are listed in Table S2.

RNA sequencing

hPSCs were seeded at the density 200k per well in a 12-well plate 24 hours before treatment. hPSCs were grown under 4 experimental conditions: untreated pluripotent cells grown in mTeSR1, hPSCs treated with WNT3a (300ng/ml) for 6 hours, hPSCs treated with WNT3a (300ng/ml) for 18 hours or hPSCs treated with CHIR (8uM) for 6 hours. Total RNA was collected with the Invitrogen RNAqueous-Micro Total RNA Isolation Kit. Processed RNA was stored at -80°C, and RNA integrity was checked by Nanodrop, agarose gel electrophoresis, and qPCR and the Agilent 2100 system. Sequencing was performed by Novogene Co. using the Illumina paired-end 150 platform (NovaSeq6000). Another biological repeat was performed using the same protocol.

Image acquisition

Imaging acquisition of fixed samples was done on an Olympus/Andor spinning disk confocal or an Olympus FV3000 confocal laser scanning microscope with a 20x, 0.75NA air objective. At least n=5, but generally n=8 (this number is specified in the legend of each figure), images were recorded for each experimental condition, acquiring either three or five z-planes spaced 2.5uM apart per position.

For live imaging experiments, reporter cell lines were maintained in antibiotic selection for the H2B fluorescent marker for at least three days and stopping 2 days before seeding, at the latest, to maximize the number of fluorescent cells in the culture. To remove any possible debris, cells were washed two times with mTeSR1 media before recording, which started at least one hour before treatment to have a pre-treatment baseline for each condition. Imaging acquisition of fixed samples was done on an Olympus/Andor spinning disk confocal with a 20x, 0.75NA air objective. Time-lapse imaging intervals were 15 minutes, and Z-stacks were acquired in three planes spaced 2.5mM apart. During imaging, temperature (37 °C), humidity (~50%), and CO_2 (5%) were controlled, and media change was performed without moving the plate from the stage. 8 positions of each condition were selected for imaging.

QUANTIFICATION AND STATISTICAL ANALYSIS

RNA sequencing quantification

To quantify the abundance of transcripts for each sample, Salmon v1.8.0 was used.[70] To align our data, we used the human transcriptome (GRCh38) index for salmon, with salmon index using the selective alignment method (salmon_sa_index:default in http://refgenomes.databio.org/v3/genomes/splash/2230c535660fb4774114bfa966a62f823fdb6d21acf138d4). We quantified transcripts with Salmon using the -l A flag to infer the library type (paired-end) automatically and the –validateMappings -o flag to use the mapping-based mode. The resulting datasets were then processed using the tximeta2 package in R[71], and the counts matrix was exported for downstream analyses in MATLAB (code available at https://github.com/warmflashlab/Camacho-Aguilar2022_BMPWNT). Datasets are deposited in Gene Expression Omnibus (GEO) repository with accession number GSE245027.

Image analysis

For analysis of fixed samples, maximum intensity projections were computed for each image. Image analysis was performed using Ilastik[72,73] for initial segmentation on the DAPI channel, and custom-written MATLAB code was used for further analysis. In the case of fixed imaging, nuclear protein expression was measured by mean nuclear intensity and normalized by mean nuclear DAPI to correct for intensity variations due to optics.

For analysis of live imaging, maximum intensity projections were computed for each image. Image analysis was performed using Ilastik[72,73] for initial segmentation using the H2B channel, and custom-written MATLAB code was used for further analysis. Smad4 dynamics was quantified as the nuclear to cytoplasmic Smad4 ratio.[39] The resulting quantified dynamics were normalized to pre-treatment levels at each position, and to the non-treated condition to generate the final quantifications.

All image processing code is available at https://github.com/warmflashlab/Camacho-Aguilar2022_BMPWNT

For the analysis of the micropatterning experiment, stitching of the colonies was performed in Fiji using the algorithm in. Preibisch et al.[74] Segmentation and mean intensity quantification were done on Ilastik[72,73] and custom software written in MATLAB (MathWorks), previously described in Warmflash et al.[17]

Cell fate classification

(see Appendix in supplemental information)

Mathematical models

(see Appendix in supplemental information)